Computations of Flow Structures and Heat Transfer in a Dimpled Channel at Low to Moderate Reynolds Number

Wilfred Vinod Patrick

Thesis submitted to the Faculty of the
Virginia Polytechnic Institute and State University
In partial fulfillment of the requirements for the degree of

Master of Science
In
Mechanical Engineering

Dr. Danesh K. Tafti, Chair
Dr. Brian Vick
Dr. Saad Ragab

April 25th, 2005
Blacksburg, Virginia

Keywords: Dimples, Concavities; DNS; Transition; Flow structure.

COMPUTATIONS OF FLOW STRUCTURE AND HEAT TRANSFER IN A DIMPLED CHANNEL AT LOW TO MODERATE REYNOLDS NUMBER

Wilfred V. Patrick

Abstract

Time-accurate calculations are used to investigate the three-dimensional flow structure and understand its influence on the heat transfer in a channel with concave indentations on one wall. A dimple depth to channel height ratio of 0.4 and dimple depth to imprint diameter ratio of 0.2 is used in the calculations. The Reynolds number (based on channel height) varies from Re = 25 in the laminar regime to Re = 2000 in the early turbulent regime. Fully developed flow and heat transfer conditions were assumed and a constant heat flux boundary condition was applied to the walls of the channel. In the laminar regime, the flow and heat transfer characteristics are dominated by the recirculation zones in the dimple with resulting augmentation ratios below unity. Flow transition is found to occur between Re = 1020 and 1130 after which both heat transfer and friction augmentation increase to values of 3.22 and 2.75, respectively, at Re = 2000. The presence of large scale vortical structures ejected from the dimple cavity dominate all aspects of the flow and heat transfer, not only on the dimpled surface but also on the smooth wall. In all cases the thermal efficiency using dimples was found to be significantly larger than other heat transfer augmentation techniques currently employed.

Acknowledgement

I am very grateful to Dr. Tafti for his infinite patience and support without which I would not have completed this important phase of my career.
Having had the pleasure of taken courses by both Dr. Vick and Dr. Ragab, I was very pleased to have them be on my committee, and would like to take this opportunity to thank them for it.
My parents, who have been all the strength and inspiration I will ever need. My friends in Blacksburg, Aroon, Evan, Giridhar, Samer, Sonia, Sumana, Sundar, Tejas and Vikram, for making my experience something I will cherish forever.

Table of Contents

Computations of Flow Structure and Heat Transfer in a Dimpled Channel at Low to Moderate Reynolds Number

List of Figures

Tables

Introduction

Extensive research effort has been focused on reducing the consumption of non-renewable energy. Improving the efficiency of the universal process of heat exchange is one such area which continues to attract a lot of attention. Enhancing the efficiency of heat transfer is useful in a variety of practical applications such as macro and micro scale heat exchangers, gas turbine internal airfoil cooling, fuel elements of nuclear power plants, powerful semiconductor devices, electronic cooling, combustion chamber liners, bio medical devices, etc. Compact heat exchangers and gas turbine internal airfoil cooling are two applications which have been the subject of study for a number of researchers over the recent years.

Compact heat exchangers are used extensively in the trucking industry as radiators to reduce the excess thermal energy. Approximately one half of the energy consumption of a truck traveling at 55 mph is used to overcome the aerodynamic drag. One of the main limitations to the aerodynamic shape of the truck is the large grill frontal area required to allow enough air to pass through the radiator for the engine to be sufficiently cooled. Improved efficiency of compact heat exchangers can permit smaller radiators leading to smaller frontal area and thus can lead to substantial fuel saving.

In a compact heat exchanger there are three important aspects of heat transfer. The first aspect to consider is the convection of heat from the fluid to the tube wall of the heat exchanger. The heat is then conducted through the walls of the tube. Finally, the heat is removed from the tube surface by convection to the air flowing through it. Air-side resistance to heat transfer in compact heat exchangers comprises between 70-80 percent of the total resistance and hence any improvement in the efficiency of a compact heat exchangers is focused on augmenting the air side convective heat transfer.

In the development of advanced turbine systems there has been considerable effort focused on increasing the inlet temperature of the turbine to augment the thermal efficiency and the specific thrust. The use of thermal barrier coating and super alloys are found to be inadequate without advanced internal cooling systems. Various cooling techniques incorporating intensifiers such as ribs and pin fins are designed to function

under the different operational conditions, to allow for higher inlet temperatures, durability, and to maintain structural integrity in gas turbines.

The most widely used method to increase the convective heat transfer is to disturb the thermal boundary layer to make it thinner or partially break it. This can be achieved by using interrupted and /or patterned extended surfaces, augmenting the surface area available for heat transfer as well as the heat transfer coefficients.

Advanced cooling systems also include "intensifiers" such as pin fins, protruding ribs (turbulators), louvered fins, offset-strip fins, slit fins and vortex generators are some commonly used examples. The choice of such intensifiers, their pattern and placements are suitably selected based on the design criteria to obtain the required cooling. These wall roughners not only periodically break the thermal boundary layers but they also cause the occurrence of wall layer agitations. The flow disturbances can lead to self sustaining instabilities which cause further enhancement in the heat transfer.

Heat transfer augmentation using these methods always results in increasing the hydrodynamic resistance that adversely affects the engine aerodynamics and cycle efficiency due to the increase in frictional losses. For example louvered fins can achieve a heat transfer augmentation between 2 to 5, the frictional losses, however, are between 4 to 10 times as great as that of an equivalent flat plate fin. Fig. 1. provides the typical heat transfer enhancement, pressure penalty and the thermal efficiency ($(Nu/Nu_o)/(f/f_o)^{1/3}$) of some representative surfaces used. In the case of cooling of turbine blades, surface protrusions induce excessive pressure losses which elevate the compressor load. The separated flow field over ribs or pin fins can induce significant non-uniform cooling leading to thermal stresses. Advanced cooling designs are also difficult to manufacture and cause an undesirable increase in the total weight of the system.

Over the past couple of years the focus on using concavities or dimples, to provide enhanced heat transfer has been documented by a number of researchers. It is evident from studies that the use of dimples not only provides enhanced heat transfer but it can overcome most of the drawbacks of the other methods employed for augmenting heat transfer. Studies by various researchers have repeatedly yielded heat transfer enhancement comparable to ribs with pressure losses of almost half that experienced

under the use of ribs, and even reduced drag coefficient in some cases – Bearman and Harvey (1993).

In using dimples the extended surface is indented instead of protruding into the flow due to which there is a considerable reduction in the pressure penalty. The heat transfer enhancement provided by dimples is comparable to most rib turbulators but slightly less than some of the complex broken rib configuration. Besides the cooling enhancement and low pressure drop, dimples make manufacturing easier and help reduce the weight of the cooling system which is of critical importance.

When the important considerations in the design of a cooling system; the cooling level required, effective cooling with minimum coolant flow, minimum drag, manufacturing cost and reduction in weight are all considered, the use of dimples have a clear and distinct advantage over the other methods employed.

A number of theories have been put forth on the mechanism by which dimples enhance surface heat transfer and the effect the dimples have on the flow which in turn results in enhanced heat transfer. Concavities serve to increase both the heat transfer surface and induce instabilities in the flow. Flow visualizations over dimples indicate that self organizing dynamic vortex structures that flow out of the cavities in the form of jets ensure intensive mass transfer into the core of the main fluid. Intensive mass transport of the heat transfer agent (fluid) from the wall region of the flow to the inner regions is the main reason for a decrease in thermal resistance in the vicinity of a heat releasing surface and therefore in heat transfer enhancement.

The use of concavities has long been recognized to cause flow benefits for a variety of applications. The pioneers of application of dimples for heat transfer enhancement are Russian researchers, whose work surfaced rather recently. Most of their work concentrates on flow and heat transfer for both a single dimple and a row of dimples in an internal channel. There are numerous experimental studies which have looked into the effect of dimples on heat transfer in internal turbine airfoil cooling. Concavity geometry, concavity shape, spacing, distribution, density and dimple depth are some of the aspects which have been studied by various researchers.

Bearman and Harvey (1993) have shown that dimples on golf balls delay boundary layer separation and subsequently reduce the drag on the dimpled ball as compared to a

smooth ball. The same investigators also studied cross flows over dimpled cylinders and determined that the drag coefficient was significantly lower for a dimpled cylinder as compared to smooth cylinder at high Reynolds number. The depth of the dimples used in these calculations was the optimum depth as found by Kimura and Tsutahara (1991).

Afanasyev et al. (1993) studied experimentally the friction and heat transfer on surfaces shaped by systems of spherical cavities streamlined by turbulent flows. Experimental data on heat transfer were generalized and a correlation of heat transfer and the geometric parameters used were obtained. The investigators attributed the heat transfer enhancement to a slight decrease in the thickness of the viscous sublayer and also the three dimensional nature of the cavities which produce a wall pressure gradient that determines the mechanism of heat transport in the region. Heat transfer enhancement of about 30-40 percent was reported without appreciable pressure losses.

Belenkiy, Gotovskiy et al. (1993) used a regular system of spherical cavities. The character of the resulting heat transfer augmentation was studied experimentally by changing the surface geometry, sizes and design of the test section at Re_H = 5,000 to 20,000. It was observed that for some cases heat transfer enhancement was accompanied by a decrease of pressure losses in comparison with a smooth surface. Maximum heat transfer enhancements of about 2.5 times were obtained.

Kezarev and Kozlov (1994) investigated the flow structure and local transfer coefficient on the surface of a hemispherical cavity. Positions of streamlines along the cavity surface resembled that of an electric dipole containing a source and a sink. The investigators found that as the free stream turbulence grew, the mean value of the heat transfer coefficient on the surface of the cavity also increased. The convective heat flux from the cavity was higher than that from the surface of a plane circle of the same diameter. Terekhov et al. (1995) have provided experimental data for measurements of flow structure, heat transfer and pressure field for a single dimple on one surface. Various magnitudes and frequencies of flow oscillations are described. The dependence of heat transfer and pressure drop on the dimple geometry is also documented. Zhak (1995) studied flow visualization and describes the variety of vortex structures in various rectangular shaped cavities.

Schukin et al. (1995) present results on heat transfer augmentation for a heated plate downstream of a single hemispherical cavity in a diffuser channel and in a convergent channel. Data on the influences of the turbulence intensity level and the angles of divergence and convergence have on heat transfer augmentation were determined and the potential of using concavities are mentioned.

Chyu et al. (1997) studied the enhancement of surface heat transfer in a channel using dimples. It was observed that the concavities served as vortex generators to promote turbulent mixing in the bulk flow to enhance the heat transfer at Re_H = 10,000 to 50,000, H/d of 0.5, 1.5, 3.0 and δ/d =0.575 (see Fig. 2.). Two different concavities – hemispheric and tear drop were used in the experiments. Heat transfer enhancement similar to that of continuous rib turbulators of 2.5 times the smooth channel values and very low pressure losses that were almost half that caused by ribs were obtained. Tear drop concavities were used in order to minimize the low heat transfer zones in the dimple cavity. It was found that although the tear drop shape consistently induced higher heat transfer than the hemispheric shape in the concavity, they resulted in similar levels of overall heat transfer augmentation of about 2.5 times the smooth channel values.

Lin et al. (1999) provide computational results for a high aspect ratio channel in which the walls are lined with four rows of hemispherical cavities arranged in a staggered fashion. The geometry and flow conditions were similar to that used by Chyu et al (1997). Re_H = 23,000 to 46,000 was used. The focus of the study was on the flow induced by cavities and the effect it had on the heat transfer. The computed results were compared with available experimental data. The k-ω turbulence model was used. Quantitatively the computed and measured results were similar for the third cavity but not for the other cavities. This discrepancy was considered to be due to the differences in the channel flow condition at the channel inlet, number of cavity rows and width of the channel (finite in experiments versus infinite in computation). Flow streamlines and temperature distribution were presented which provided insight into the flow structure.

Park et al. (2004) examined turbulent air flow in a channel with deep dimples (δ/d = *0.3*) numerically using the realizable k-ε model for Re_H = 2,700 to 41,000. This study provided insight into the development of flow structures produced by the dimples and

their subsequent impact on heat transfer. However, the predicted heat transfer augmentation patterns and values were not in good agreement with experiments.

Moon et al. (1999) investigated experimentally the effect of channel height on heat transfer and friction in a rectangular dimpled passage with dimples on one wall. The geometry used was H/d = 0.37, 0.74, 1.11, 1.49 and Re_H = 12,000 to 60,000. They discovered a Nusselt number augmentation of about 2.1 for $0.37<H/d<1.49$. It was found that the heat transfer augmentation was invariant with the Reynolds number. The increase in friction factor was 1.6 to 2.0 times the smooth channel value. The thermal performance of the dimples was superior to that of continuous ribs. Neither the heat transfer coefficient distribution nor the friction exhibits any detectable dependence the channel height for the studied relative height range.

Acharya and Zhou (2001) focused on heat transfer enhancement with dimples produced in rotating turbine blades. The experiments were performed in test apparatus designed for the study of mass transfer (sublimation of naphthalene). Mass transfer measurements presented the surface distribution of the Sherwood number from which the Nusselt number was obtained. The results of this study indicated that there was not much variation between the stationary and rotation values.

Bunker and Donnellan (2003) present details about heat transfer and friction factor for flows inside circular tubes with concavity arrays at Re_D = 20,000 to 90,000 with fully turbulent flow and δ/d = 0.2 to 0.4. The results yielded heat transfer augmentation of 2 or more for $\delta/d > 0.3$ and high dimple density. This study provides the first insight into the heat transfer and friction effects for various concavity arrays for turbulent flows.

Moon and Lau (1999) experimentally studied the convective heat transfer and pressure drop for turbulent airflow in a square channel with a dimpled wall with Re_H = 10,000 to 65,000. Nine different concave and cylindrical cavities were studied with various dimple depths and diameters. It was observed that the dimple depth was an important parameter which had a direct relation to the heat transfer enhancement. It was also observed that the cylindrical dimples had a higher heat coefficient based on the projected area and lower pressure drop than that of the concave dimples of similar geometry.

Mahmood and Ligrani (2002) experimentally analyzed the influence of dimple aspect ratio, temperature ratio, Reynolds number and flow structures in a dimpled channel at Re_H = 600 to 11,000 and air inlet stagnation temperature of 0.78 to 0.94. with H/d =0.20, 0.25, 0.5, 1.00. The results indicated that the vortex pairs which are periodically shed from the dimples become stronger as channel height decreases with respect to the imprint diameter.

Mahmood et al. (2001) studied the heat transfer in a channel with dimples on one side and protrusions on the other with a channel aspect ratio of 16. H/d = 0.5 and Re_H = 5,000 to 35,000. It was found that because of the additional vortical secondary flows and flow structures induced by the protrusions the Nusselt numbers were considerably augmented and had a greater dependence on the Reynolds number. But there was also a considerable increase in the friction factor which caused the thermal efficiency to be less than the channel without protrusions. Ligrani et al. (2002) also studied the flow structures and local Nusselt number variations in a channel with dimples and protrusion on opposite walls for aspect ratio of 16, H/d = 0.5 and Re_H = 380 to 30,000. Instantaneous flow visualization images and surveys of time averaged flow structure show that the protrusion result in added vortical, secondary flow structures and flow mixing. It was observed that more mixing resulted at lower Reynolds number when protrusions where used. It was seen that 2 sets of vortices develop in the cavities in both halves which periodically move upwards in a burst thereby increasing the mixing and enhancing heat transfer.

The objective of this paper is to study the low to moderate Reynolds number flow regime typical of compact heat exchangers, which is not found in the experimental nor the computational literature. This regime spans laminar steady, transitional, and low Reynolds number turbulent flow. Of primary interest is the heat transfer and friction augmentation characteristics and the role of both steady and unsteady coherent vorticity. To resolve the transitional and low Reynolds number turbulent characteristics of the flow, Direct Numerical Simulations (DNS) is employed. An additional calculation of the highest Reynold flow was done using the Large Eddy Simulation (LES) model. The calculations presented here are unique in a number of respects: in extending the state-of-the-art in the application of time-dependent CFD to complex geometries; in studying the transitional and low Reynolds number turbulence regime which has not been studied before for this

geometry; and finally leading to an enhanced understanding of heat transfer augmentation over dimpled surfaces by resolving the spatio-temporal evolution of flow variables.

Nomenclature

d	imprint diameter
D	concavity diameter
$\vec{e}_x$	unit vector in x-direction
f	Fanning friction factor
H	channel height (characteristic length)
h	heat transfer coefficient
k	thermal conductivity (W/mK)
L_x	length of domain in x-direction
$\vec{n}$	surface normal vector
Nu	Nusselt number, hH/k
p	transverse pitch and fluctuating pressure
Pr	Prandtl number ($\mu C_p / k$). Pr = 0.7
Q_x	mean flow in x-direction
q''	constant heat flux boundary condition
Re_τ	Reynolds number based on friction velocity, $u_\tau H / \nu$
Re, Re_H	Reynolds number based on bulk velocity, $\bar{u}_b H / \nu$
s	streamwise pitch
T	Temperature
$\vec{u}$	Cartesian velocity vector
$\bar{u}_b$	mean bulk flow velocity
u_τ	friction velocity
$\vec{x}$	physical coordinates
β	mean pressure gradient
δ	dimple depth
δ_{ij}	Kronecker delta
γ	mean temperature gradient
θ	fluctuating, modified or homogenized temperature

Ω total heat transfer surface area

$\vec{\xi}$ computational coordinates

Subscripts

s surface

b bulk

0 smooth channel

Computational model and governing equations

The computational model assumes fully-developed flow and heat transfer and simulates a periodically repeating spatial unit as shown in Fig. 2(a). The geometry consists of a channel, with dimples or concave indentations on one wall. The geometry of the dimpled pattern is defined by a streamwise pitch *s*/H** =3.24, transverse pitch *p*/H**=3.24, imprint diameter *d*/H**=2.0, diameter *D*/H**=2.9, and depth δ^*/H^*=0.4, where *H** is the channel height. These parameters were selected for optimum heat transfer augmentation based on past experimental studies**.** Both channel walls are heated by imposing a constant heat flux (*q"*) boundary condition. The governing flow and energy equations are non-dimensionalized by a characteristic length scale which is chosen to be the height of the channel (*H*), a characteristic velocity scale given by the friction velocity $u_\tau = \sqrt{\Delta \bar{P}_x / \rho}$, and a characteristic temperature scale given by $q" D_h / k$. Fully-developed flow requires the assumption of periodicity, the assumed periodicity of the domain in the streamwise or *x*-direction requires that the mean gradients of pressure and temperature be isolated from the fluctuating periodic component as follows:

$$P(\vec{x},t) = P_{in} - \beta x + p(\vec{x},t)$$
$$T(\vec{x},t) = T_{in} + \gamma x + \theta(\vec{x},t) \qquad (1)$$

On substitution into the Navier-Stokes and energy equations, the *non-dimensional* time-dependent equations in transformed coordinates $\vec{\xi} = \vec{\xi}(\vec{x})$ take the following conservative form[1]:

Continuity:

$$\frac{\partial}{\partial x_j}\left(\sqrt{g}U^j\right) = 0 \qquad (2)$$

Momentum:

$$\frac{\partial}{\partial t}\left(\sqrt{g}u_i\right) + \frac{\partial}{\partial \xi_j}\left(\sqrt{g}U^j u_i\right) = -\frac{\partial}{\partial \xi_j}\left(\sqrt{g}(\vec{a}^j)_i p\right)$$
$$+ \frac{\partial}{\partial \xi_j}\left(\left(\frac{1}{\mathrm{Re}_\tau}\right)\sqrt{g}g^{jk}\frac{\partial u_i}{\partial \xi_k}\right) + \sqrt{g}\beta\delta_{i1} \qquad (3)$$

[1] Henceforth, all usage is in terms of non-dimensionalized values.

Energy:

$$\frac{\partial}{\partial t}\left(\sqrt{g}\theta\right)+\frac{\partial}{\partial \xi_j}\left(\sqrt{g}U^j\theta\right)= \frac{\partial}{\partial \xi_j}\left(\left(\frac{1}{\Pr \mathrm{Re}_\tau}\right)\sqrt{g}\,g^{jk}\,\frac{\partial \theta}{\partial \xi_k}\right)-\sqrt{g}\gamma u_1 \tag{4}$$

where $\vec{a}^i$ are the contravariant basis vectors[2], $\sqrt{g}$ is the Jacobian of the transformation, g^{ij} are the elements of the contravariant metric tensor, $\sqrt{g}U^j=\sqrt{g}(\vec{a}^j)_i u_i$ is the contravariant flux vector, $\bar{u}_i$ is the Cartesian velocity vector, and θ is the modified temperature.

The mean pressure gradient β is assumed to be unity, whereas γ is calculated from a global energy balance as: $\gamma = q''\Omega / \mathrm{Re}_\tau \Pr Q_x L_x$. The boundary conditions imposed on the channel walls are as follows:

$$\begin{aligned} &\vec{u}=0 \\ &\nabla p\cdot\vec{n}=0 \\ &\nabla\theta\cdot\vec{n}=1-\gamma\vec{e}_x\cdot\vec{n} \end{aligned} \tag{5}$$

and in the streamwise and spanwise direction as:

$$\phi(x+L_x, z+L_z)=\phi(x,z); \phi=\vec{u},\, p,\quad and\quad \theta. \tag{6}$$

The governing equations for momentum and energy are discretized with a conservative finite-volume formulation using a second-order central difference scheme on a non-staggered grid topology. For the time advancement of the discretized continuity and momentum equations, a projection method is used. The temporal advancement is performed in two steps, a predictor step, which calculates an intermediate velocity field, and a corrector step, which calculates the updated velocity at the new time step by satisfying discrete continuity. The energy equation is advanced in time by the predictor step. The computer program GenIDLEST (**Gen**eralized **I**ncompressible **D**irect and **L**arge-**E**ddy **S**imulations of **T**urbulence) used for these simulations has been applied extensively to study air-side heat transfer augmentation in compact heat exchangers [Zhang and Tafti (2001); Tafti and Zhang (2001); Cui and Tafti (2002)] and other

[2] The notation $\left(\vec{a}^j\right)_k$ is used to denote the *k-th* component of vector $\vec{a}^j$. $(\vec{a}^j)_k = \partial\xi_j / \partial x_k$

applications. Details about the algorithm, functionality, and capabilities can be found in Tafti (2001).

A hybrid structured/unstructured multi-block grid is used to discretize the computational domain with a total mesh resolution of 1.22 million computational cells. The 104 block mesh is shown in Figure 3(b). It is designed such that maximum resolution is provided in the dimple, and in the vicinity of the top and bottom surfaces. In the wall normal direction the first grid point is placed at Δ = 0.005 in the dimple and the bottom channel surface, and 0.01 at the top smooth channel wall. Maximum mesh spacing in the cross-stream direction is set at 0.1 at the channel center. Hence in an average sense, at the highest Reynolds number of Re_τ= 280, the first grid point lies at 1.4 wall units in the dimple and the bottom wall, and 2.8 wall units at the top wall.

Typically the calculations are initiated with some initial guess of the velocity and temperature field under the imposed pressure gradient and integrated in time till the flow and heat transfer adjust to the new conditions and reach a steady state. In the unsteady regime, when the flow develops self-sustaining instabilities, the velocity and temperature fields are integrated further to obtain statistical means. Typical sampling times are 3 to 5 non-dimensional time units. The mean fields are then used to present time-averaged data.

To characterize the heat transfer, we define a local Nusselt number based on channel height as

$$Nu = \frac{H \quad q'' \quad /(T_s^* - T_{ref}^* \,)}{\kappa} \tag{7}$$

where T_s^* and T_{ref}^* are the dimensional surface temperatures and global reference temperature respectively. In terms of non-dimensional quantities the above can be re-written as

$$Nu = \frac{1}{\theta_s - \theta_{ref}} \tag{8}$$

where θ_s is the local modified non-dimensional surface temperature and θ_{ref} is the reference modified non-dimensional temperature, which is defined as:

$$\theta_{ref} = \frac{\iint |u| \theta dA_x}{\iint |u| dA_x} \tag{9}$$

The surface-averaged Nusselt number is obtained by integration over the channel and dimple surface as:

$$Nu = \frac{\iint \ dS}{\iint (\theta - \theta_{ref})dS} \tag{10}$$

where S denotes the heat transfer surface.

The Fanning friction coefficient f is calculated as:

$$f = \frac{2\Delta p^{*}(2H)}{4\rho L_x^{*}\bar{u}^{*2}_b} \tag{11}$$

In non-dimensional form the expression reduces to

$$f = \frac{1}{\bar{u}_b^2} \tag{12}$$

where $\bar{u}_b$ is the bulk flow velocity obtained from the simulation under the condition of the applied mean pressure gradient of unity.

The heat transfer and friction augmentation ratios are calculated based on the laminar baseline values in a plane channel given by:

$$Nu_o = 4.12 \tag{13}$$

and

$$f_o = 12/\mathrm{Re}_H\,. \tag{14}$$

Results and Discussion

Calculations are presented for seven different Reynolds numbers Re_τ = 15, 55, 80, 110, 155, 225, and 280, which result in Re = 25, 280, 570, 1020, 1130, 1600 and 2000, spread over the laminar and transitional flow regimes in a smooth channel. First, the dominant flow structure is presented in terms of instantaneous and mean coherent vorticity distributions. This is then related to the wall shear stress and heat transfer augmentation. The friction factor and the Nusselt number obtained for all the cases are tabulated in Table 1. The calculation denoted by 2000t used the dynamic Smagorinsky model [Germano et al., 1991]

A. Flow Structures

Fig. 4 shows the mean streamline distribution at different Reynolds numbers in the center plane of the dimple. At the lowest Reynolds number, Re = 25, there is no flow separation and recirculation in the dimples, whereas in all the other cases the flow in the dimple is characterized by a recirculation zone within the dimple. The flow separates at the leading edge of the dimple and the separated shear layer is drawn into the dimple cavity where it reattaches downstream. As the Reynolds number increases, the recirculation zone gains in strength and extends further downstream in the dimple before reattachment until *Re* =1020. At Re=1020, the flow begins to develop asymmetries and soon transitions to a chaotic state at Re=1130. Because of the unsteady flow, at Re= 2000 there is a substantial shrinkage in the recirculating zone due to the increased mixing and transfer of momentum. Heat transfer is highest at the downstream rim of the dimples where the flow reattaches. The recirculation zone is characterized by the smallest heat transfer coefficients.

In order to understand the unsteady nature of the flow and the associated vorticity dynamics the $\nabla \boldsymbol{u}$ vortex identification technique is used to educe coherent vorticity (Chong et al., 1990). This frame-invariant method identifies vortical structures as regions of large vorticity, where rotation dominates over strain to cause the rate-of-deformation tensor $\nabla \boldsymbol{u}$ (velocity gradient tensor) to have complex eigenvalues (one real and two conjugate complex eigenvalues). The complex eigenvalues imply that the local streamline pattern is closed or spiral, thus correctly eliminating near-wall shear layers. This methodology can also be separately applied in the *x*-, *y*-, or *z*- planes in order to identify streamwise, cross-flow, and spanwise vortices (Zhang et al. 1997**),** respectively. The strength of the vortex is measured in terms of the imaginary part of the eigenvalue of the velocity gradient tensor. The strength of the three components, streamwise, cross-flow, and spanwise vortices is measured in terms of the imaginary part of the eigenvalue of the velocity gradient on the *x*-, *y*-, and *z*- planes, respectively.

Fig. 5 depicts an isosurface of the instantaneous coherent vorticity on the dimpled surface. In the laminar regime the vorticity is concentrated symmetrically about the dimple centerline at the upstream and downstream edges of the dimples. At Re = 1020,

asymmetries appear in the distribution of coherent vorticity in the reattachment region. At Re = 1130, the flow transitions to an unsteady state and vorticity generation increases in the reattachment region. By Re = 2000, the rate of generation of vorticity is much higher. Vorticity in the reattachment region is now ejected out of the dimple into the main flow at a much more regular rate.

Fig. 6 shows the time-averaged coherent voriticity distribution for two planes one near the top (y = 0.97) and the other near the bottom (y = 0.05) of the channel. The weak coherent vorticity located near the top surface is notably influenced by the dimples in the steady regime at *Re* = 280 and 570 and exhibit a close similarity to the dimple pattern. The magnitude of vorticity is maximum near the downstream and upstream rim of the dimple which is a manifestation of the expansion of flow into the dimple cavity at the upstream edge and subsequent contraction at the downstream edge. At higher Reynolds number, however, the vorticity distribution appears to exhibit a streaky pattern of alternating high and low magnitudes, similar to that observed in the wall region of turbulent boundary layers. However, since these are time-averaged distributions, the streaks which are observed are hypothesized to be a consequence of the dimples at the bottom wall. However, no clear pattern with respect to the dimpled surface is discernable.

Near the bottom dimpled surface, at low Reynolds numbers in the steady regime most of the vorticity is concentrated above the downstream rim of the dimple and is approximately an order of magnitude larger than that near the top wall. In the unsteady regime (*Re* = 1600 and 2000) however, the coherent vorticity is more distributed and is concentrated at the downstream half of the dimple and at the downstream rim.

The distribution of total coherent vorticity in a vertical plane passing through the centerline is shown in Figure 7. At Re = 280, the vorticity is concentrated in the separated shear layer and near the upstream and downstream edge of the dimple. The distribution is similar at Re = 1020. After transition at Re = 2000, high vorticity is concentrated in the downstream half of the dimple and also on the flat landing between dimples**.** High values are also found in the vicinity of the top wall.

Fig. 8 shows the volume averaged (over the whole computational domain) magnitude of *x*-, *y*-, *z*- coherent vorticity components and the total coherent vorticity. At *Re* = 280, the z- component of vorticity has the highest magnitude. The *z* component of vorticity is

very localized and found mostly at the rims of the dimples, just before the fluid is drawn into the dimple cavity and just after reattachment of the separated shear layer as the flow emerges from the dimple. As the Reynolds number increases to 1020, just before the development of flow instabilities, both the *x*- and *y*- directional vorticity components are more prevalent in the dimple cavity with weak traces of the *y*- directional vorticity extending up to the top surface of the channel. As the flow becomes unsteady, there is a sharp increase in all three components of vorticity. As at lower Reynolds numbers, *z*-vorticity is highly localized near the downstream rim of the dimples. Now unsteady vortical structures are ejected out of the dimple in the downstream half from the region of reattachment. These structures are initially predominantly aligned with the *y*-direction but change orientation as they come in contact with the external flow. These vortices are by and large responsible for heat transfer augmentation downstream of the dimple.

Figure 9 plots frequency spectrum of streamwise velocity fluctuations at Re = 1600 at a location downstream of the dimple. A characteristic peak is observed at a non-dimensional frequency (based on H and $\bar{u}_b$) of 0.032. Park et al. (2002) for Re = 20,000 yielded a primary vortex shedding frequency of 8.0 Hz. or a non-dimensional frequency of 0.11. The difference is attributed to the large difference is Reynolds number between the two cases.

B. Shear Stress and Friction

Fig. 10 shows the normalized surface stress (τ_{xy}/τ_{xy0}) distribution on the top and bottom surfaces of the channel. τ_{xy0} indicates the shear stress in a smooth channel of height H. Nominally, the top wall of the channel should exhibit a uniform value of unity, however as seen earlier in the vorticity distribution, the presence of dimples on the bottom surface perturbs the shear stress distribution. At steady flow conditions, the predominant effect comes from the flow expansion and contraction. At higher Reynolds numbers in the unsteady regime, the augmentation pattern is much more complicated and exhibits an alternating streaky structure of high and low augmentation ratios. On the bottom dimpled surface, the negative surface stresses in the dimples are due to the recirculation zone. The negative stress results in lowering the friction penalty of dimpled surfaces at low Reynolds numbers keeping the overall ratio below unity. However, as the Reynolds number increases into the unsteady regime, surface stresses increase dramatically.

The overall friction coefficient is shown in Fig. 11 (a) together with the laminar and turbulent variation in a smooth channel. **(**Fig. 11(b) shows the augmentation ratio compared to a smooth laminar channel flow. At Re = 25, dimples result in more than 20% reduction in friction factor relative to a straight channel. At this Reynolds number, there is no flow separation in the dimples and the reduction in friction factor is a consequence of the effective increase in cross-sectional area and the reduction in velocity gradients at the wall[3]. At Re = 280, the combined effect of flow recirculation, which contribute a negative shear stress, and the change in flow geometry result in a 10% reduction in friction over that of a smooth channel. As the Reynolds number increases, there is gradual increase in friction coefficient till it reaches a value close to unity at Re = 1020. Thus in the laminar regime, dimples have the potential to be used effectively to reduce friction on non heat transfer regions. Once the flow transitions with the development of flow oscillations, there is a large increase in the friction coefficient, and the augmentation ratio increases from 1.75 at Re = 1130 to 3.25 at Re = 2000.

[3] In all cases, the friction factor is calculated using equation (11), which is based on the hydraulic diameter of a straight channel.

C. Heat Transfer

The various flow phenomena caused by using the concave cavities have a significant impact on the surface heat transfer. The recirculating flow in the dimples, generation of vortical structures, fluid outflow from the cavities at higher Reynolds numbers, are all responsible for resolving the surface heat transfer, not only on the dimpled surface but also on the non-dimpled surface.

Fig. 12 shows the instantaneous coherent vorticity distribution together with the heat transfer distribution at the dimpled surface for Re = 2000. There is a clear correlation between the vortices and the surface heat transfer. A region of high heat transfer exists in the reattachment region within the dimple. The outflow of fluid in the form of elongated streamwise vortices moving over the bottom surface correlate to the instantaneous high heat transfer regions.

Fig. 13 shows the normalized Nusselt number distribution for the dimpled surface. The Nusselt number is normalized by using the baseline value of Nusselt number of a smooth laminar channel flow. As established by various researchers, maximum heat transfer occurs near the downstream rim of the dimples in all cases. The recirculating flow in the dimple is responsible for poor heat transfer in the cavity itself. At Re = 280, 570, 1020, 1130, and 1600, the heat transfer in the upstream half of the cavity is below steady smooth channel values. The region of maximum heat transfer at low Reynolds numbers begins at the reattachment of the shear layer, where the fluid impinges on the dimple wall and extends down the smooth channel as well, with a maximum magnitude of about 1.2 for Re = 280. This region of maximum heat transfer shrinks in size but grows in magnitude with increasing Reynolds number to a maximum of about 9 times the smooth channel value as in the case of Re = 2000.

Fig. 14 shows the normalized Nusselt number distribution on the top wall. Notably, there is a clear correlation between the heat transfer distribution and the dimples. At Re=25, the augmentation ratio is below unity in the region directly in line with the dimples because of flow expansion and recovers to values near unity between dimples. At *Re* = 280, the pattern changes with augmentation ratios being less affected by the presence of the dimples on the opposite wall. The augmentation decreases again as

Re increases to 570 and then increases again at *Re* = 1020. This can be attributed to the increasing effect of the dimpled wall on heat transfer as the Reynolds number increases. Maximum values occur between dimples along the centerline. As the Reynolds number increases, the pattern quickly assumes the streaky elongated structure very similar to that found in the distribution of surface shear stress and coherent vorticity, with alternating high and low augmentation ratios.

Fig. 15 plots the averaged heat transfer coefficients. Fig. 15(a) compares the overall Nusselt number with laminar and turbulent smooth channel correlations**.** Fig 15(b) plots the augmentation ratio over laminar channel flow. The overall heat transfer on the dimpled surface is less than unity in magnitude at *Re* = 280, 570 and 1020 and a maximum of 3.35 at *Re* = 2000. On the top surface, a maximum augmentation ratio of 2 is obtained at the highest Reynolds number of 2000. The maximum augmentation ratio at Re = 2000 is 1.53 based on the turbulent flow correlation.

Fig. 16 (a) shows the experimental results of the surface Nusselt number augmentation by Burgess et al. [2000] at Re = 17,200 for a dimpled channel. Fig. 16 (b) shows the numerical results at Re = 17,200 by Ligrani et al. [2002] using a realizable k-ε model for a similar dimple geometry using the commercial software Fluent. There are large differences in the distribution as well as the magnitude of heat transfer augmentation. While the maximum augmentation is measured to be 4x immediately downstream of the dimple, the predicted values only reach a value of 2.3. Not only is the augmentation underpredicted by more than a 100%, the augmentation patterns are completely different.

As a comparison, the predictions in this study compare very well with the experiments in spite of the large difference in Reynolds numbers. Fig. 16 (c) shows the current calculations which have been normalized by a turbulent Nusselt number using the Dittus-Boelter correlation. Unlike the calculations of Park et al. [2002], the predicted augmentation pattern agrees very well with the experiments. In addition, in spite of the large difference in Reynolds number, the quantitative predictions of augmentation ratios are also of a much higher quality.

Summary and Conclusion

Time-accurate simulation techniques are performed in a channel with concave cavities on one wall. The dimple geometry (s^*/H^* =1.62, p^*/H^*=1.62, d^*/H^*=2.0, D^*/H^*=2.9, and δ^*/H^*=0.4) was selected based on past studies to optimize the heat transfer. Calculations are presented for flows at low to moderate numbers (steady to transitional flow) for Re = 25, 280, 570, 1020, 1130, 1600 and 2000.

In the laminar flow regime (Re $\leq$ 1020), the flow and heat transfer on the dimpled surface is dominated by the effective increase in cross-sectional area and the reduction in velocity gradients at the wall and by the steady recirculation zones in the dimples. As a result, both friction and heat transfer are attenuated to below their nominal plain channel values. At the lowest Reynolds number, Re = 25, both the friction and heat transfer coefficients are 20% lower than in an equivalent channel. At Re = 280, the friction coefficient and Nusselt numbers are 90% and 85%, respectively of the nominal values. Transition from laminar to the chaotic or unsteady regime is found to occur between Re=1020 and 1130. At Re = 1130, there is a large increase in the friction and heat transfer augmentation ratio to 1.75 and 1.45, respectively. At Re = 2000, augmentation ratios of 3.5 and 2.75 are obtained for friction and heat transfer, respectively, and show no signs of asymptoting to a constant value.

The presence of dimples not only affects the flow and heat transfer at the dimpled surface of the channel but also at the smooth surface. At low Reynolds numbers the effect is mostly communicated through the flow expansion and contraction caused by the dimples. After transition, large scale coherent vorticity which is shed from the dimple cavity take on an active role in influencing friction and heat transfer at the top wall. Both, heat transfer augmentation patterns and surface shear stress exhibit a streaky elongated structure, similar to that exhibited by coherent vorticity in the vicinity of the surface. The bulk of the vortical structures are produced in the dimple cavity in the reattachment region. These structures on emerging from the dimple align themselves predominantly with the flow direction and are mostly responsible for heat transfer augmentation on the dimpled surface as well as the upper smooth wall as they convect downstream and enhance mixing.

References

Afanasyev, V. N., Chudnovsky, Ya. P, Leontiev, A. I., and Roganov, P. S., Turbulent Flow Friction and Heat Transfer Characteristics for Spherical Cavities on a Flat Plate, *Experimental Thermal and Fluid Science*, 7, 1-8, 1993.

Bearman, P. W., and Harvey, J.K., Control of Circular Cylinder Flow by the Use of Dimples, *AIAA Journal*, Vol. 31, 1753-1756, 1993.

Belen'kiy, M. Y., Gotovskiy, M. A., Lekakh, B. M., Fokin, B. S., and Dolgushin, K. S., Heat Transfer Augmentation Using Surfaces Formed by a System of Spherical Cavities, *Heat Transfer Research*, Vol. 25, 196-203, 1993.

Burgess, N. K., Oliveira, M. M. Ligrani, P. M., Nusselt Number Behavior on Deep Dimpled Surfaces Within a Channel, *J. Heat Transfer*, Vol. 125, 1-8, 2003.

Bunker, R. S., Donnellan, K. F., Heat Transfer and Friction Factor for Flows inside Circular Tubes with Concavity Surfaces, ASME Turbo Expo, Atlanta, paper GT-2003-38053, 2003.

Chen, J., Muller-Steinhagen, H., Duffy, G. G., Heat transfer enhancement in dimpled tubes, *Applied Thermal Engineering*, Vol. 21, 535-547, 2001.

Chong, M. S., Perry, A. E. and Cantwell, B. J., A general classification of three-dimensional flow fields, *Physics of Fluids A* 2(5), pp. 765-777, 1990.

Chyu, M. K., Yu, Y., Ding, H., Downs, J. P., Soechting, F. O., Concavity Enhanced Heat Transfer in an Internal Cooling Passage, *International Gas Turbine & Aeroengine Congress & Exhibition*, paper 97-GT-487, 1997.

Cui, J., and Tafti, D.K., Computations of flow and heat transfer in a three-dimensional multilouver fin geometry, *Int. J. Heat Mass Transfer*, Vol. 45(25), pp. 5007-5023, 2002.

Germano, M., Piomelli, U., Moin, P., and Cabot, W.H., A dynamic subgrid-scale eddy viscosity model, *Phys. Fluids*, vol. 3, pp. 1760-1765, 1991.

Griffith, T. S., Al-Hadhrami, L., Han, J.C., Heat Transfer in Rotating Rectangular Cooling Channels (AR=4) With Dimples, ASME Turbo Expo, Amsterdam, paper GT-2002-30220, 2002.

Kesarev, V. S., and Kozlov, A. P., Convective Heat Transfer in Turbulized Flow Past a Hemispherical Cavity, *Heat Transfer Research*, Vol. 25, 156-160, 1993.

Kim, Y. W., Arellano, L., Vardakas, M., Moon, H. K., Smith, K. O., Comparison of Trip-Strip/Impingement /Dimple Cooling Concepts at High Reynolds Numbers, ASME Turbo Expo, Atlanta, paper GT2003-38935, 2003.

Kimura, T., and Tsutahara, M., Fluid Dynamic Effects of Grooves on Circular Cylinder Surface, *AIAA Journal*, Vol. 29, No. 2, 2062-2068, 1991.

Kovalenko, G. V., and Khalatov, A. A., Fluid Flow and Heat Transfer Features at a Cross-Flow of Dimpled Tubes in a Confined Space, ASME Turbo Expo, Atlanta, paper GT2003-38155, 2003.

Ligrani, P. M., Harrison, J. L., Mahmood, G. I., and Hill, M. L., Flow structure due to dimple depressions on a channel surface, *Physics of Fluids* Vol. 13, No. 11, 3442-3451, 2001.

Ligrani, P. M., Mahmood, G. I., Harrison, J. L., Clayton, C. M., Nelson, D. L., Flow structure and local Nusselt number variations in a channel with dimples and protrusions on opposite walls, *Int. J. Heat Mass Transfer* 44, 4413-4425, 2001.

Lin, Y.-L., and Shih, T. I-P., Chyu, M. K., Computations for Flow and Heat Transfer in a Channel with Rows of Hemispherical Cavities, International Gas Turbines and Aeroengine Congress and Exhibition, paper 99-GT-263, 1999.

Mahmood, G. I., Hill, M. L., Nelson, D. L., Ligrani, P. M., Local Heat Transfer and Flow Structure on and above a Dimpled Surface in a Channel, ASME Turbo Expo, paper 2000-GT-230, 2000.

Mahmood, G. I., Ligrani, P. M., Heat Transfer in a dimpled channel: combined influences of aspect ratio, temperature ratio, Reynolds number, and flow structure, *Int. J. heat Mass Transfer* 45, 2011-2020, 2002.

Mahmood, G. I., Sabbagh, M. Z., Ligrani, P. M., Heat Transfer in a Channel with Dimples and Protrusions on Opposite Walls, *J. Thermophysics and Heat Transfer*, Vol. 15, No. 3, 275-283, 2001.

Moon, H. K., O'Connell, T., and Glezer, B., Channel Height Effect on Heat Transfer and Friction in a Dimpled Passage, *International Gas Turbine & Aeroengine Congress & Exhibition*, paper 99-GT-163, 1999.

Moon, H. K., O'Connell, T., and Sharma, R., Heat Transfer Enhancement using a Convex-Patterned Surface, ASME Turbo Expo, Amsterdam, paper GT-2002-30476, 2002.

Moon, S. W., Lau, S. C., Turbulent Heat Transfer Measurements on a Wall with Concave and Cylindrical Dimples in a Square Channel, ASME Turbo Expo, paper GT-2002-30208, 2002.

Park, J., Desam, P.R., and Ligrani, P. M., Numerical Predicitions of Flow Structures above a Dimpled Surface in a Channel, *Numerical Heat Transfer*, Vol. 45, 1-20, 2004

Schukin, A. V., Kozlov, A. P., and Agachev, R. S., Study and Application of Hemispheric Cavities for Surface Heat Transfer Augmentation, International Gas Turbines and Aeroengine Congress Exposition, Houston, paper 95-GT-59, 1995.

Syred, N., Khalatov, A., Kozlov, A., Shchukin, A., Agachev, R., Effect of Surface Curvature on Heat Transfer and Hydrodynamics within a Single Hemispherical Dimple, *Journal of Turbomachinery*, Vol. 123, 609-613, 2001.

Tafti, D.K., GenIDLEST – *A Scalable Parallel Computational Tool for Simulating Complex Turbulent Flows*, *Proc. ASME Fluids Engineering Division*, FED – vol. 256, ASME-IMECE, New York, 2001.

Tafti, D. K. and Zhang, X. Geometry effects on flow transition in multilouvered fins — onset, propagation, and characteristic frequencies, *Int. J. of Heat Mass Transfer* 44, pp. 4195-4210, 2001.

Terekhov, V. I., Kalinina, S. V., and Mshvidobadze, Y. M., Flow Structure and Heat Transfer on a Surface With a Unit Hole Depression, *Engineering. Thermophysics.*, *5*, pp. 11-33, 1995.

Zhak, V.D., The Taylor-Goertler Vortices and Three-Dimensional Flow Evolution in Cavity, *Russian Journal of Engineering Thermophysics*, Vol. 5, pp 165-176

Zhang, L. W., Balachandar, S. and Tafti, D. K., Effect of intrinsic three dimensionality on heat transfer and friction loss in a periodic array of parallel plates, *Numerical Heat Transfer, Part A*, 31, pp. 327-353, 1997.

Zhang, X. and Tafti, D. K., Classification and effects of thermal wakes on heat transfer in multilouvered fins, *Int. J. of Heat Mass Transfer*, 44, pp. 2461-2473, 2001.

Table 1. Summary of friction and heat transfer results

Re	***f***	***Nu***
25	0.4022	7.08
280	0.0378	6.94
570	0.0210	7.23
1020	0.0115	7.63
1130	0.0106	12.41
1600	0.0197	17.26
2000	0.0195	22.66
2000-t	0.0205	23.00

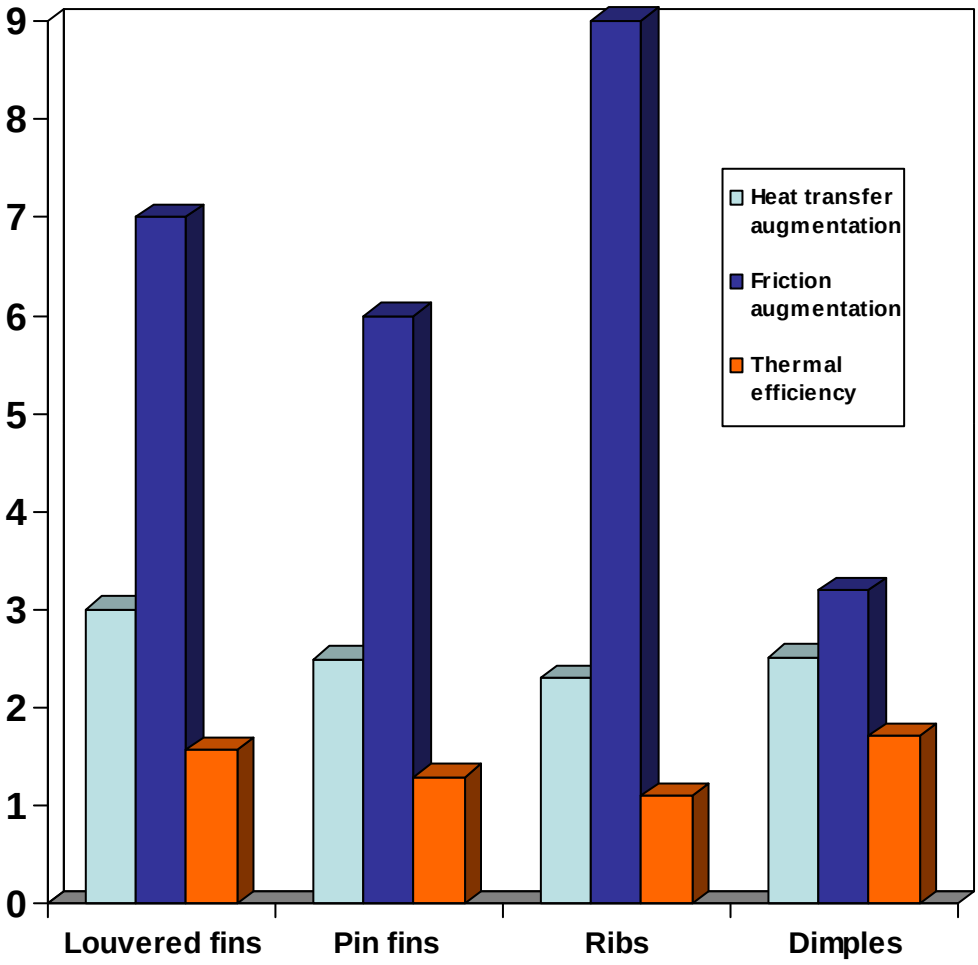

Figure 1. Thermal Efficiency of various heat transfer techniques

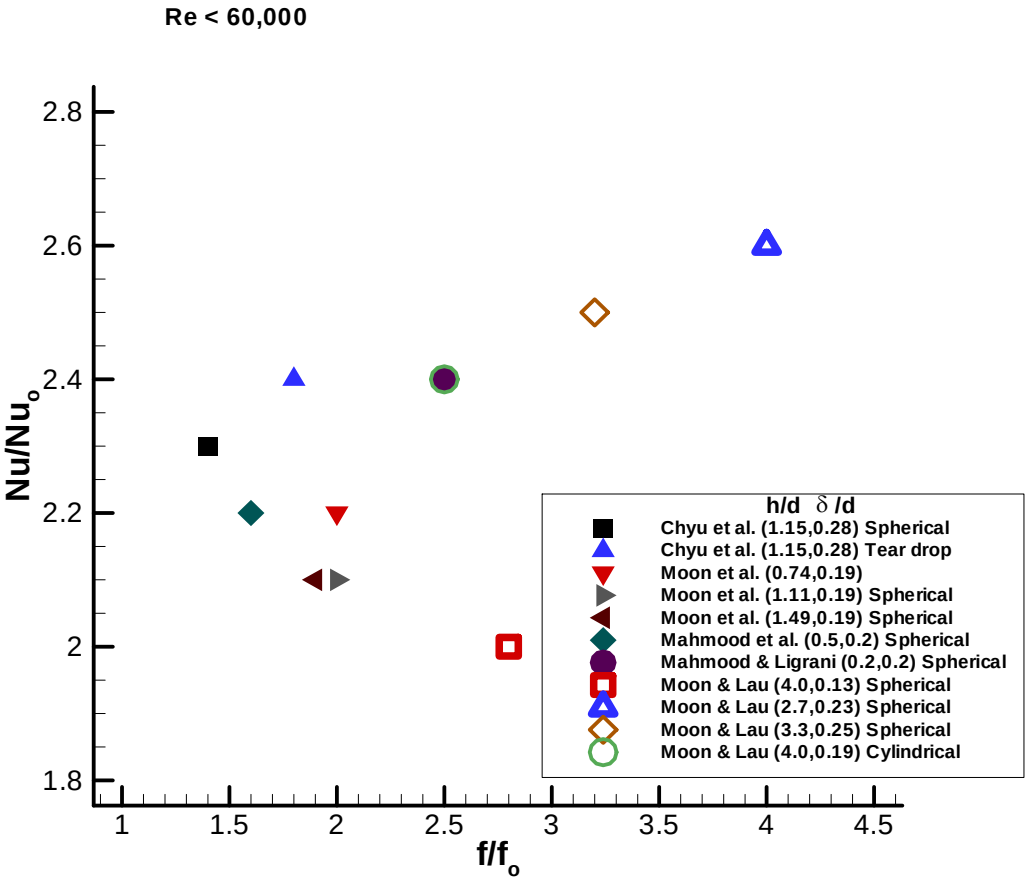

Figure 2. Past results of calculations on dimples by various researchers

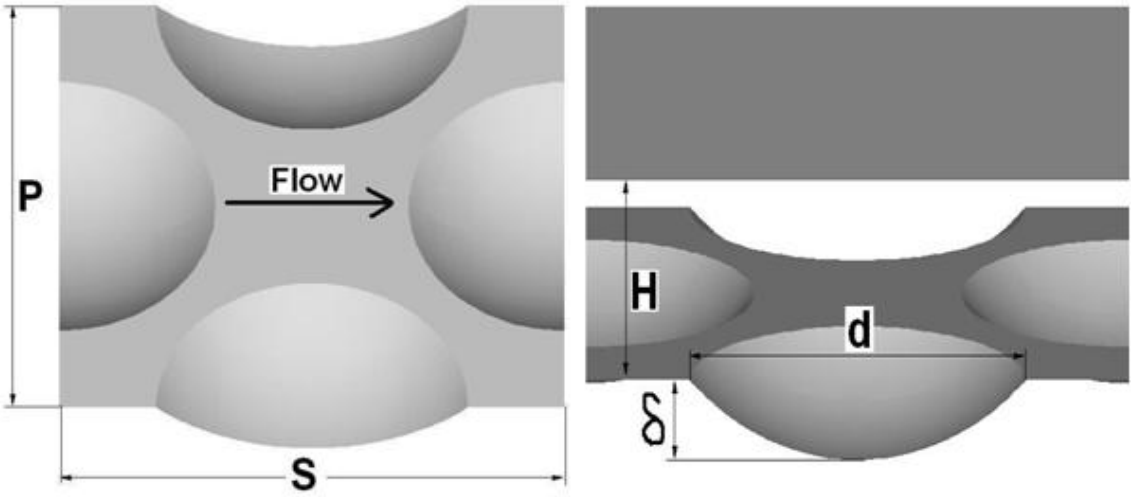

(a)

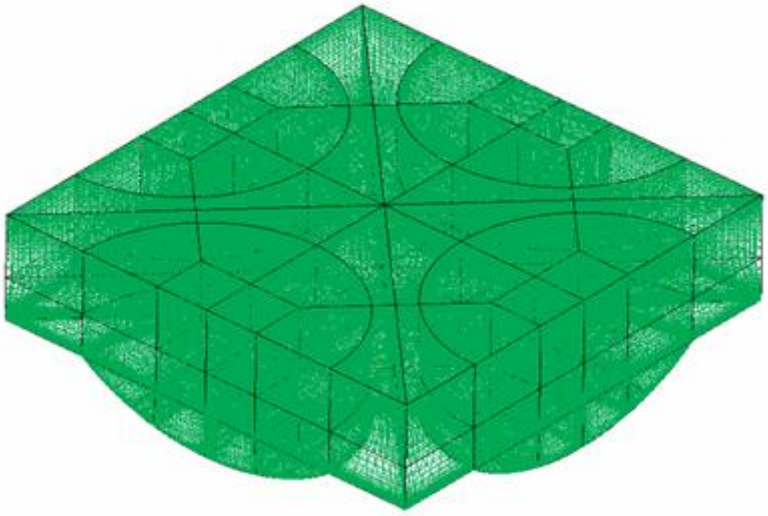

(b)

Figure 3. Dimple Geometry and mesh. The mesh consists of 104 unstructured blocks with a total resolution of 1.22 million computational cells

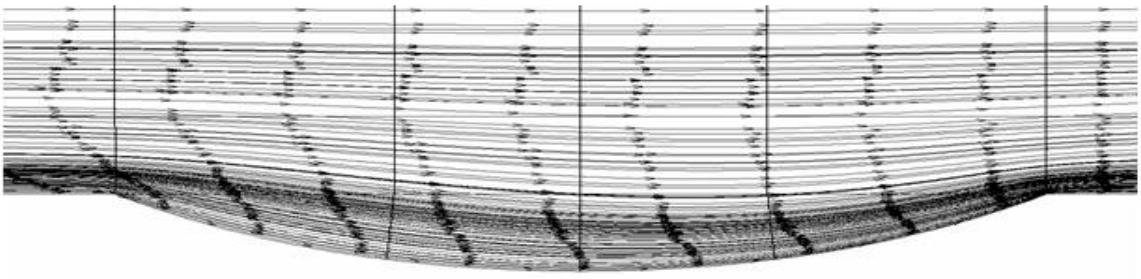

$Re_H = 25$

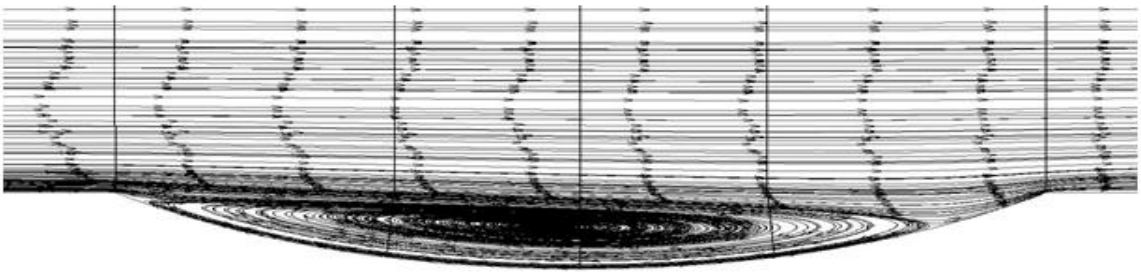

$Re_H = 280$

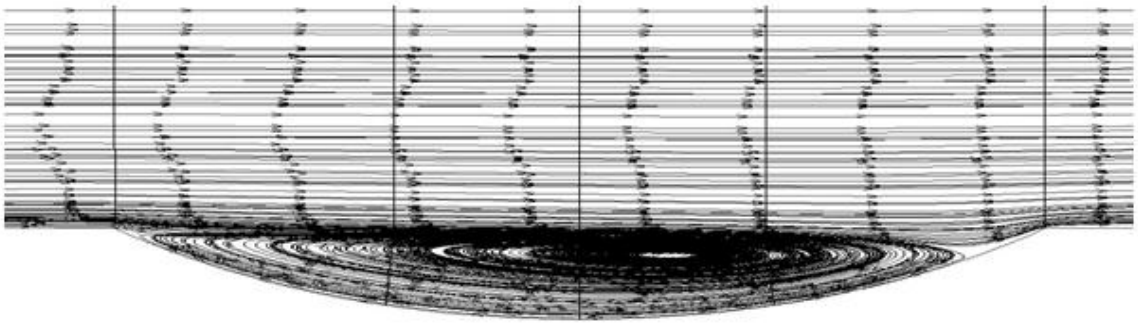

$Re_H = 570$

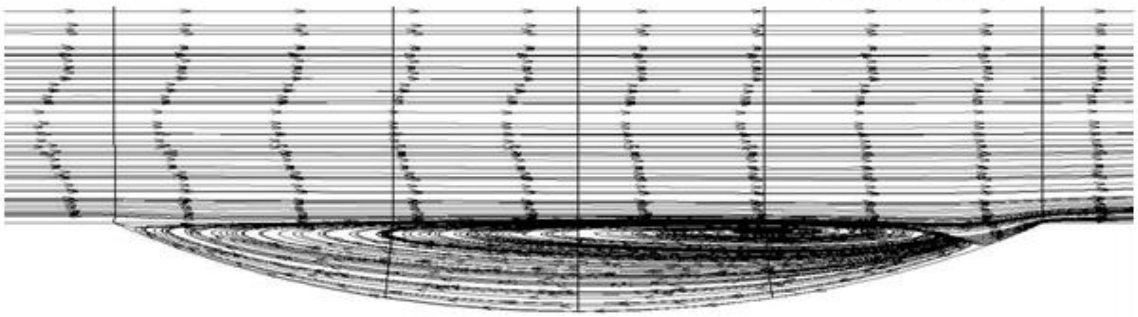

$Re_H = 1020$

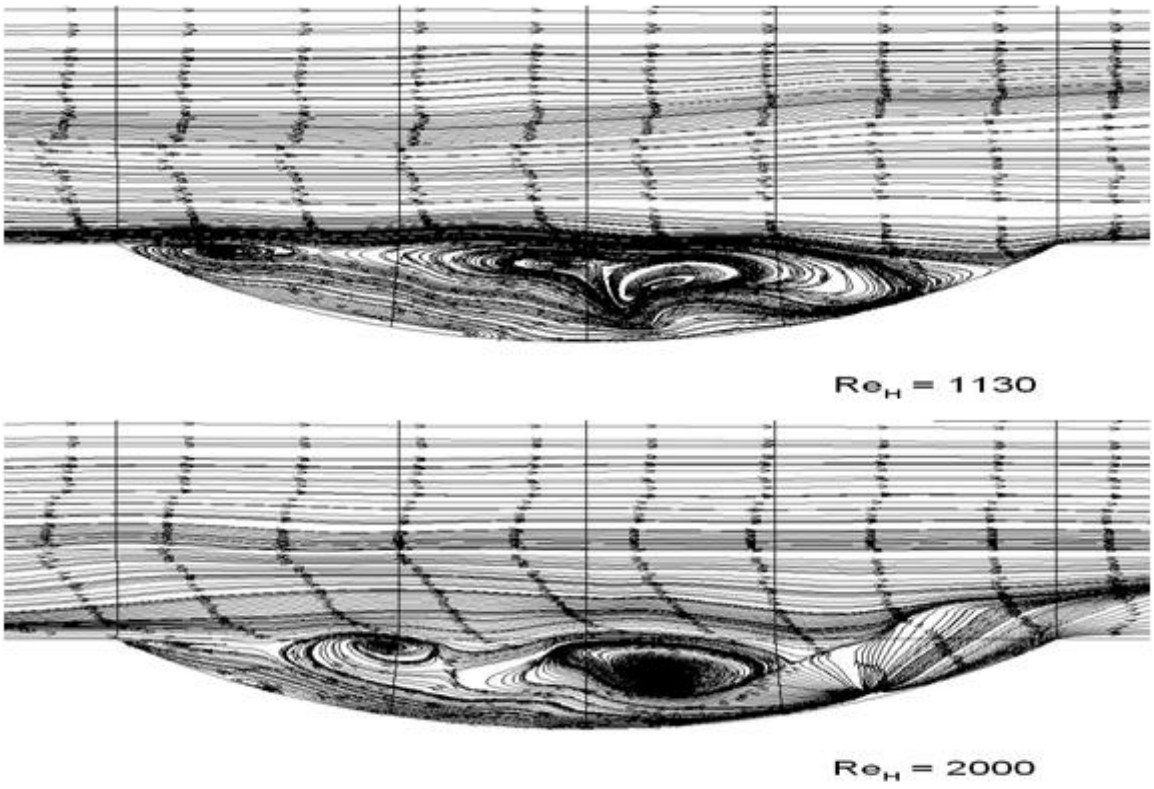

Figure 4. Mean streamline distribution in the center plane of the dimple.

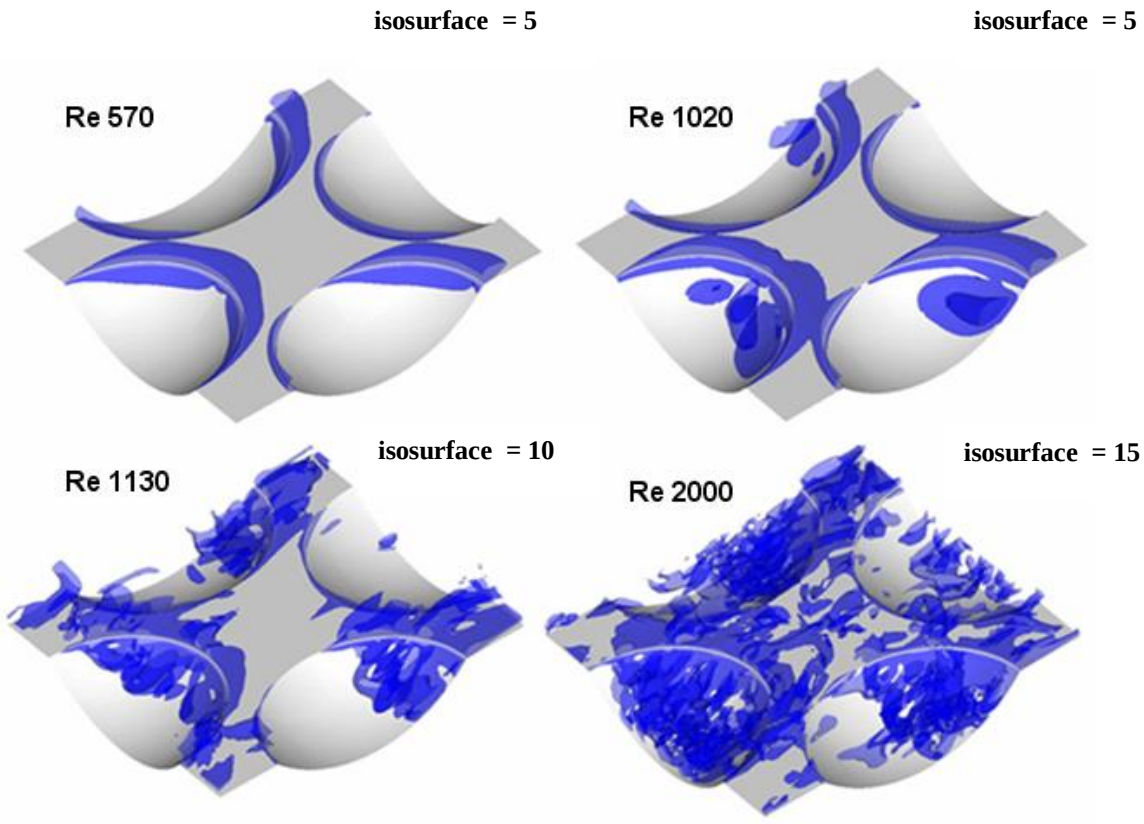

Figure 5. Isosurfaces of instantaneous coherent vorticity.

Top Bottom

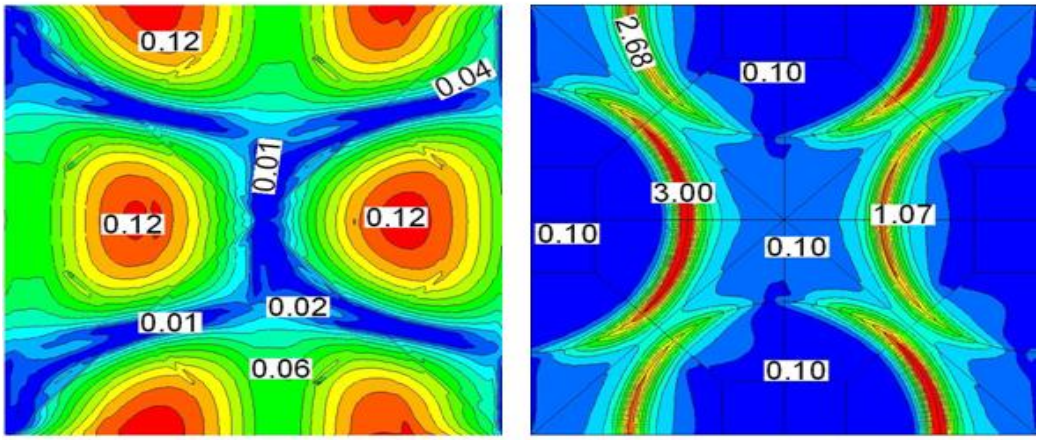

$Re = 25$

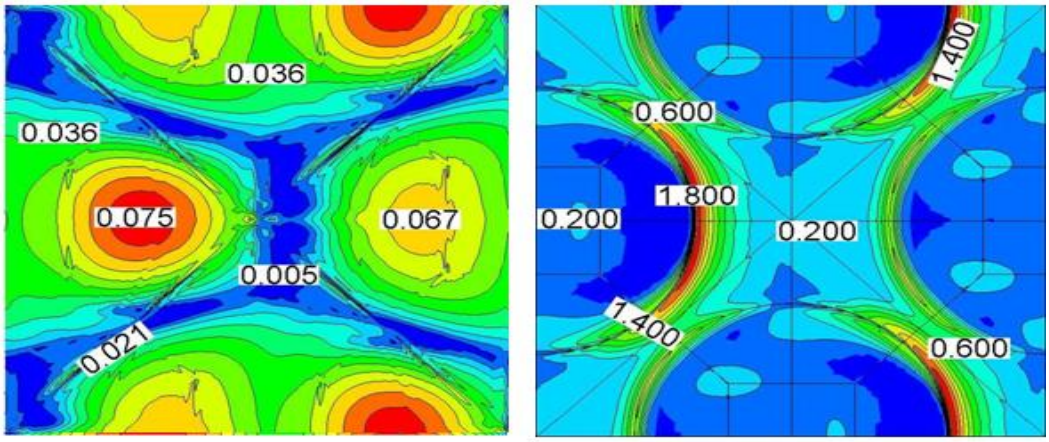

$Re = 280$

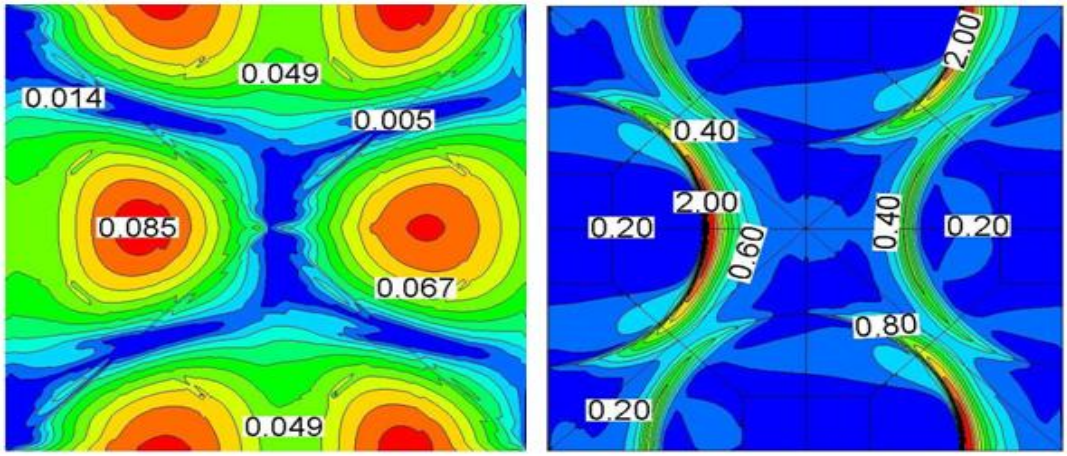

$Re = 570$

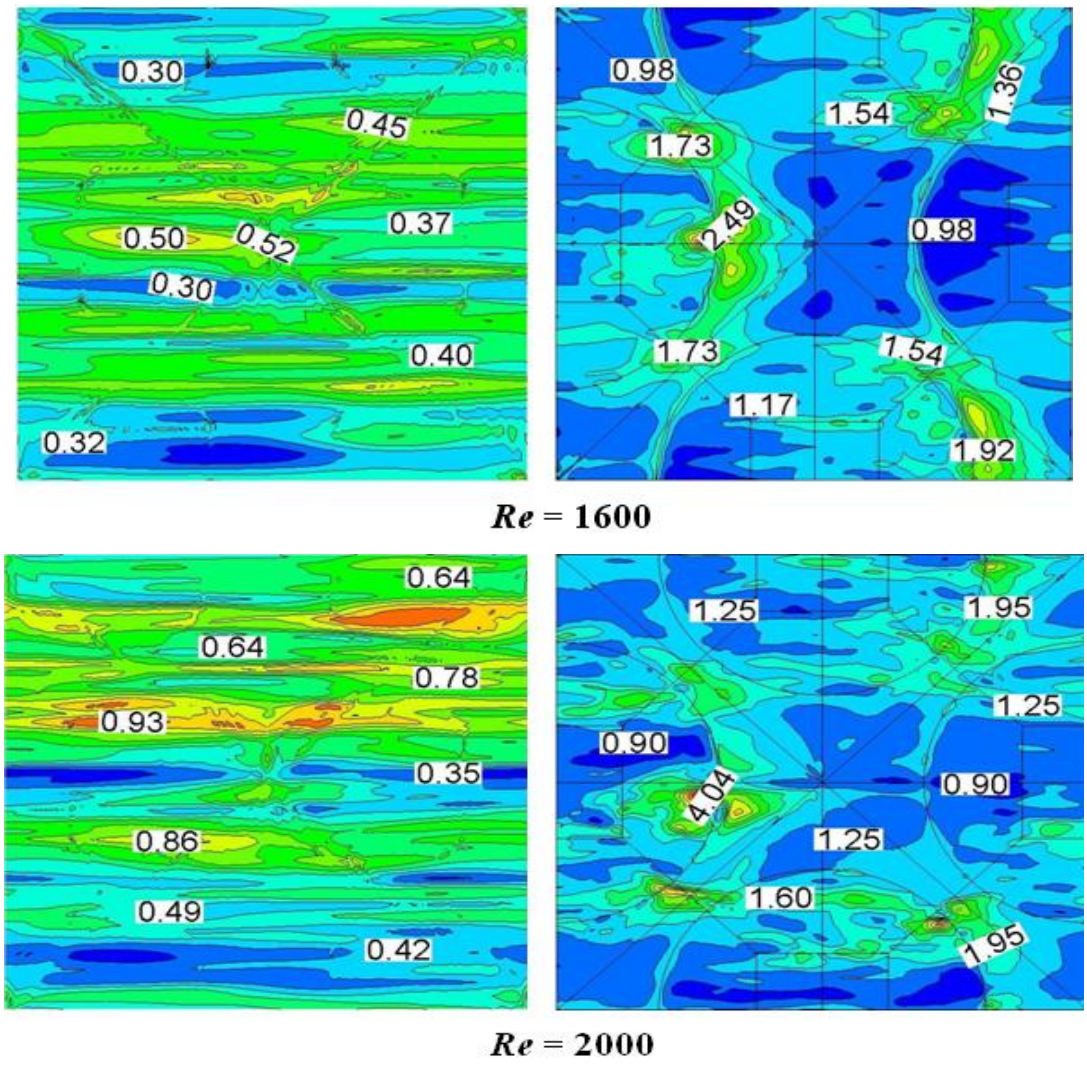

Figure 6. Total time-averaged coherent voriticity distribution on planes near the top and bottom channel surfaces.

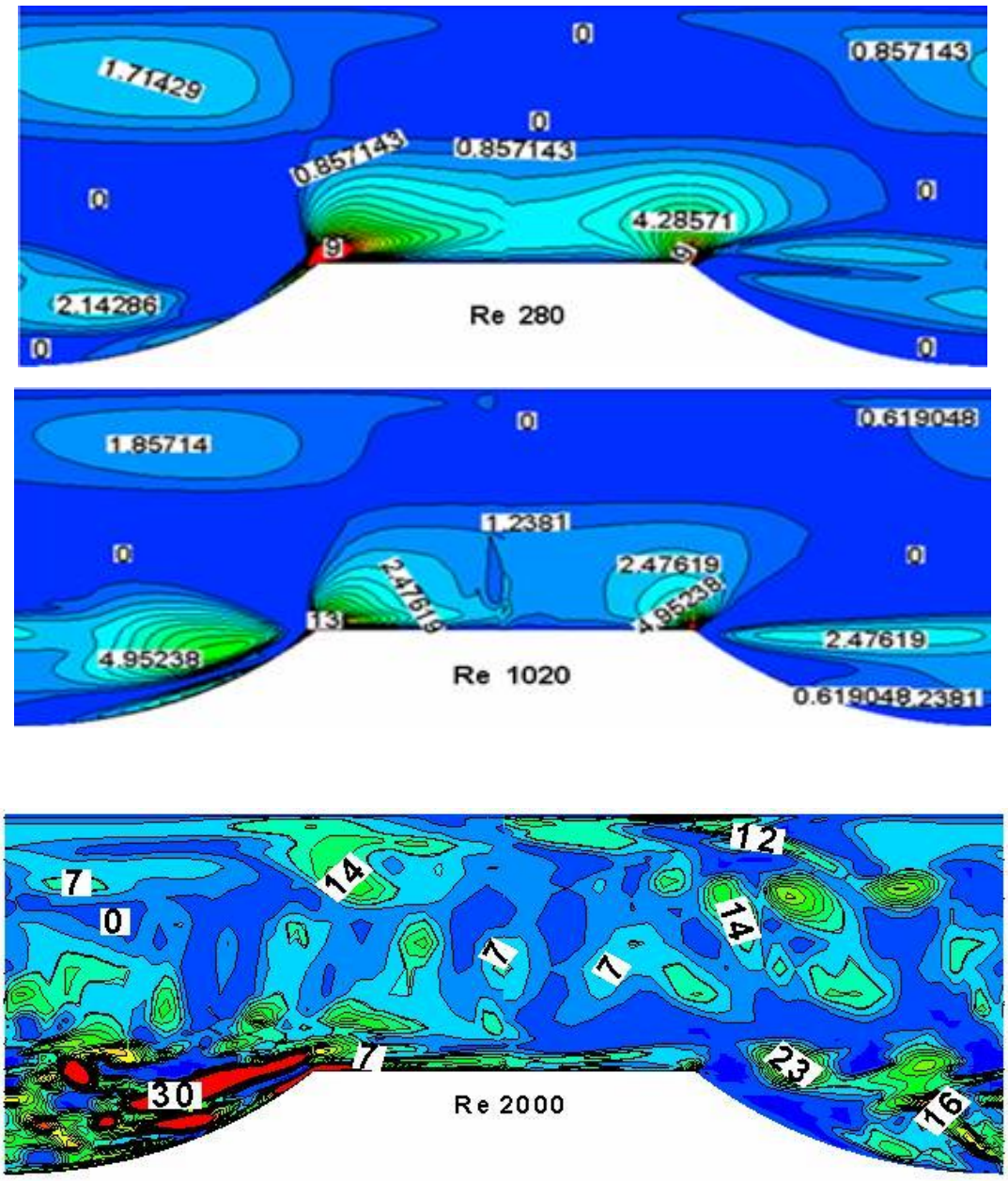

Figure 7. Total time-averaged coherent vorticity along dimple centerline across height of channel.

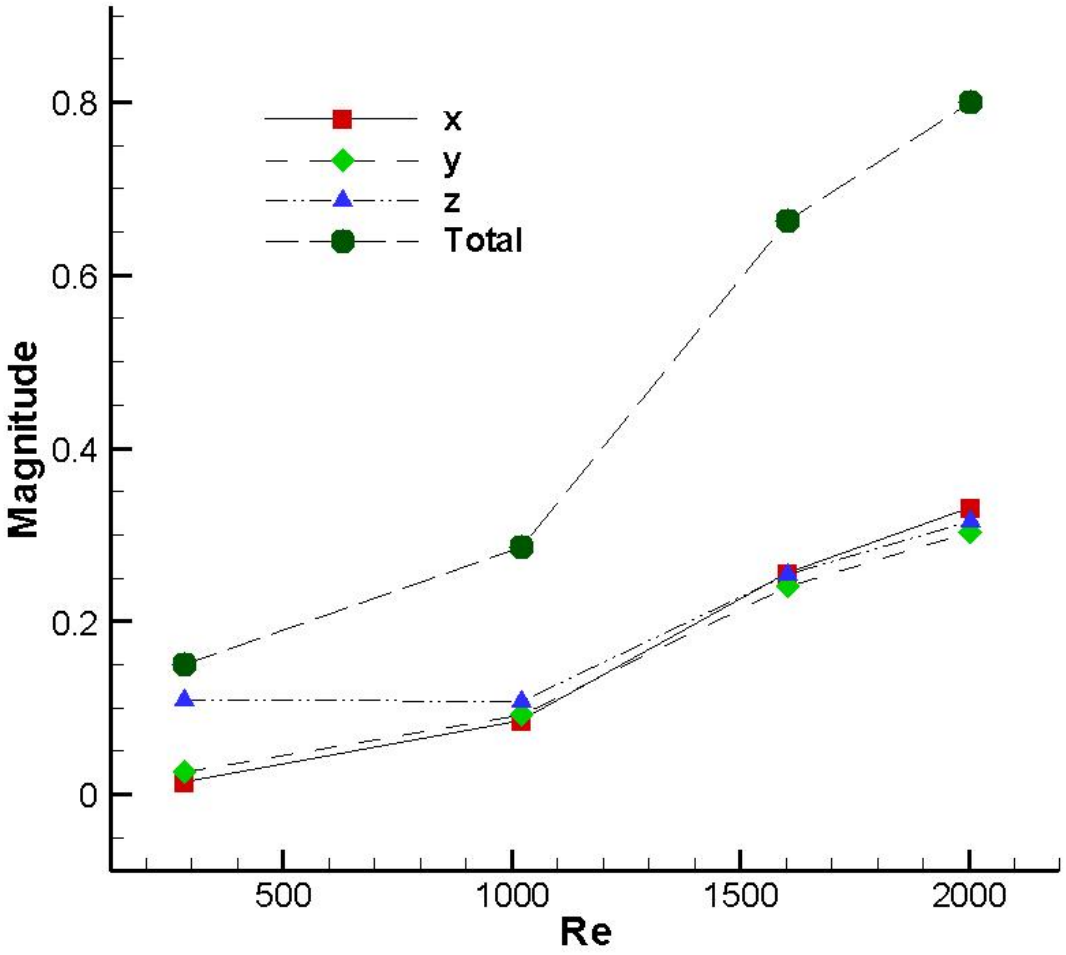

Figure 8. Volume averaged components of x-y-z and total coherent vorticity normalized by the bulk velocity.

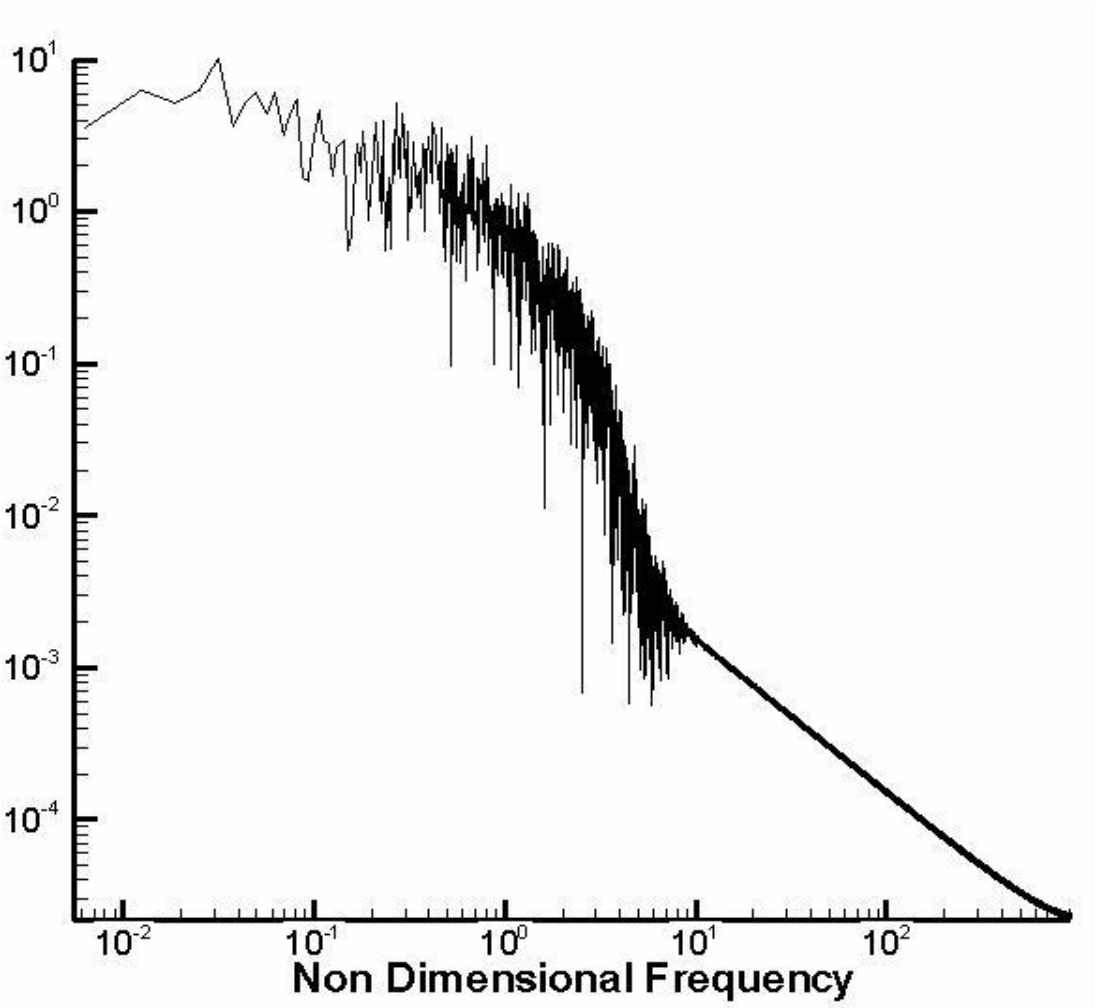

Figure 9: Frequency spectrum at Re=1600.

Top Bottom

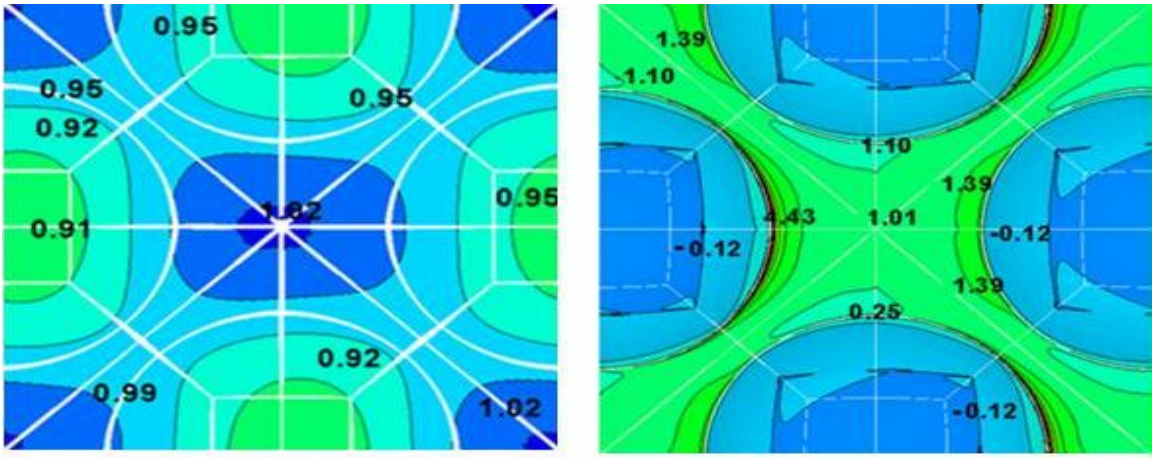

***Re* = 280**

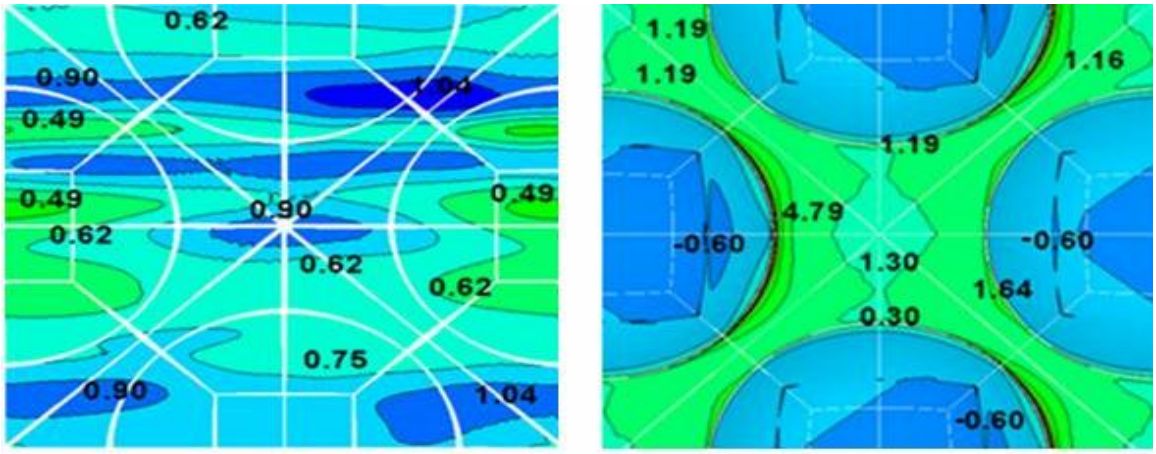

***Re* = 570**

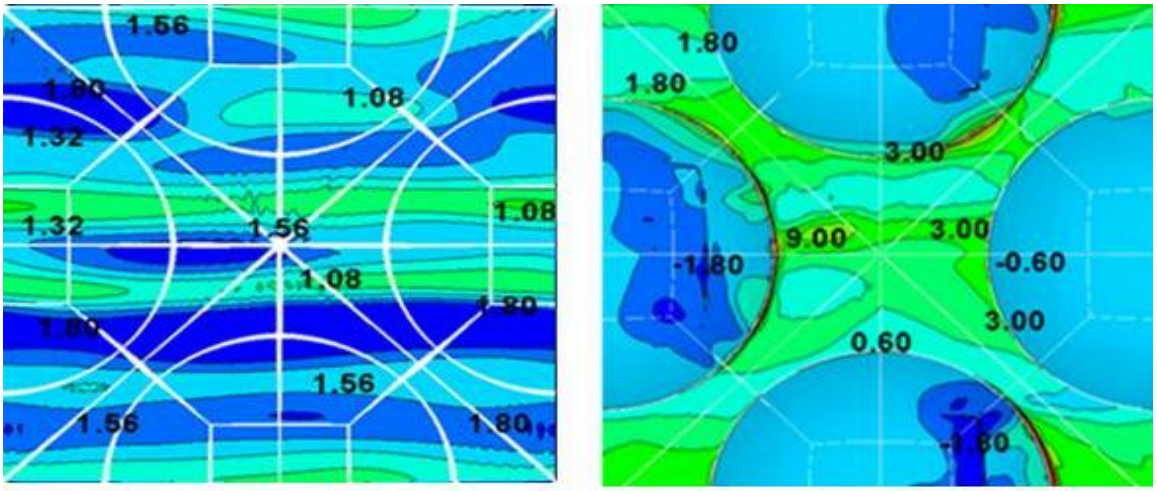

***Re* = 1130**

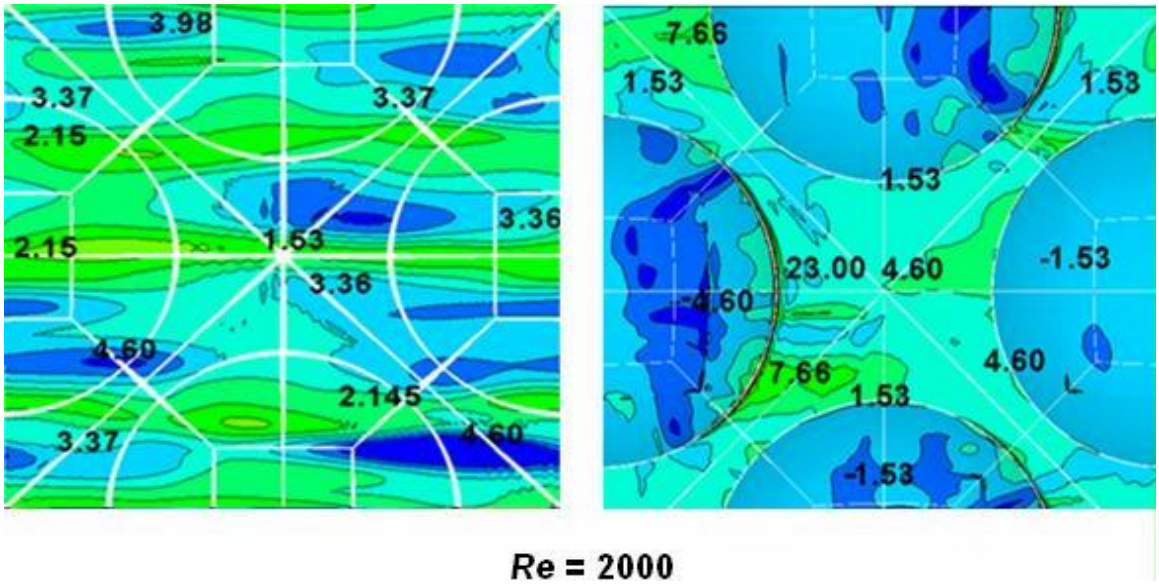

Figure 10. Normalized surface stress distribution (τ_{xy}/τ_{xy0}) on top and bottom surfaces.

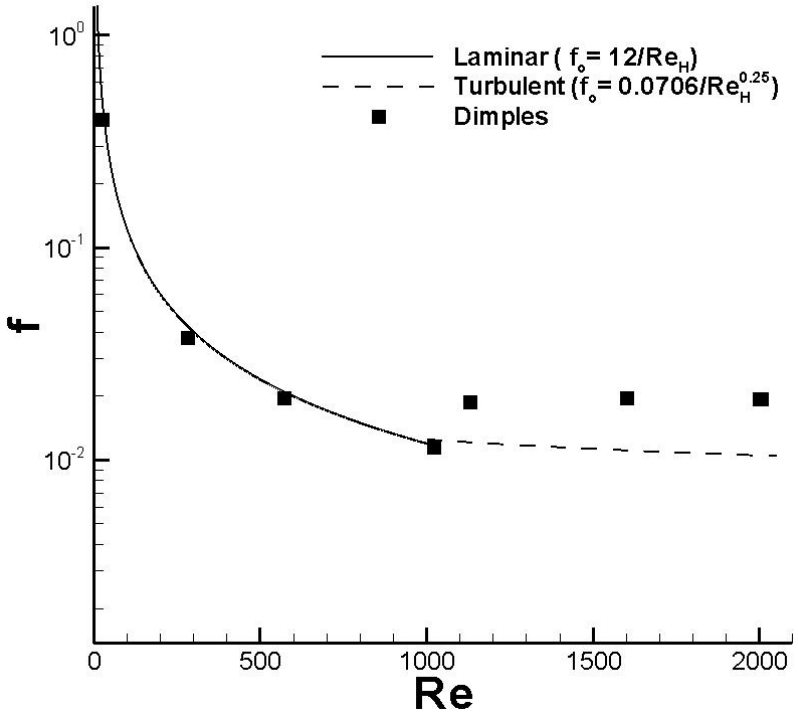

(a)

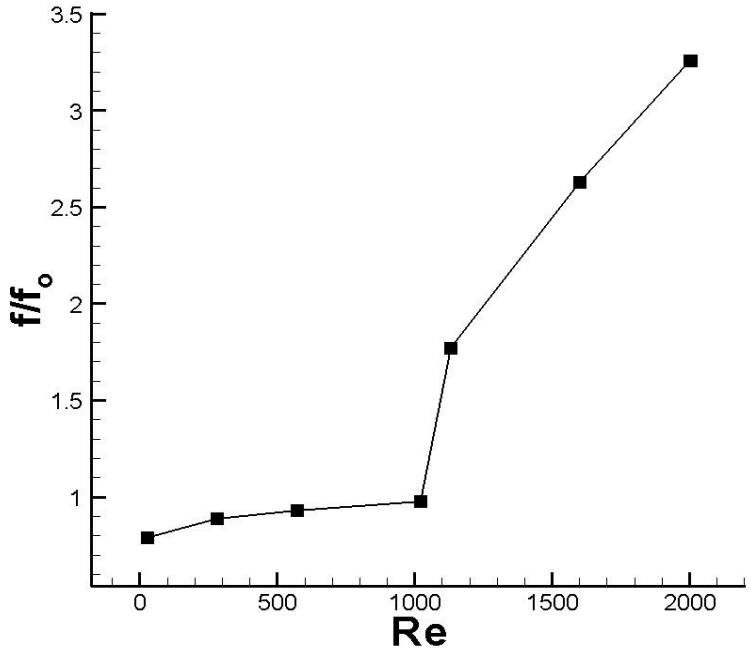

(b)

Figure 11. (a) Predicted friction coefficient compared to laminar and turbulent flow correlations. (b) Friction augmentation ratio based on laminar channel flow.

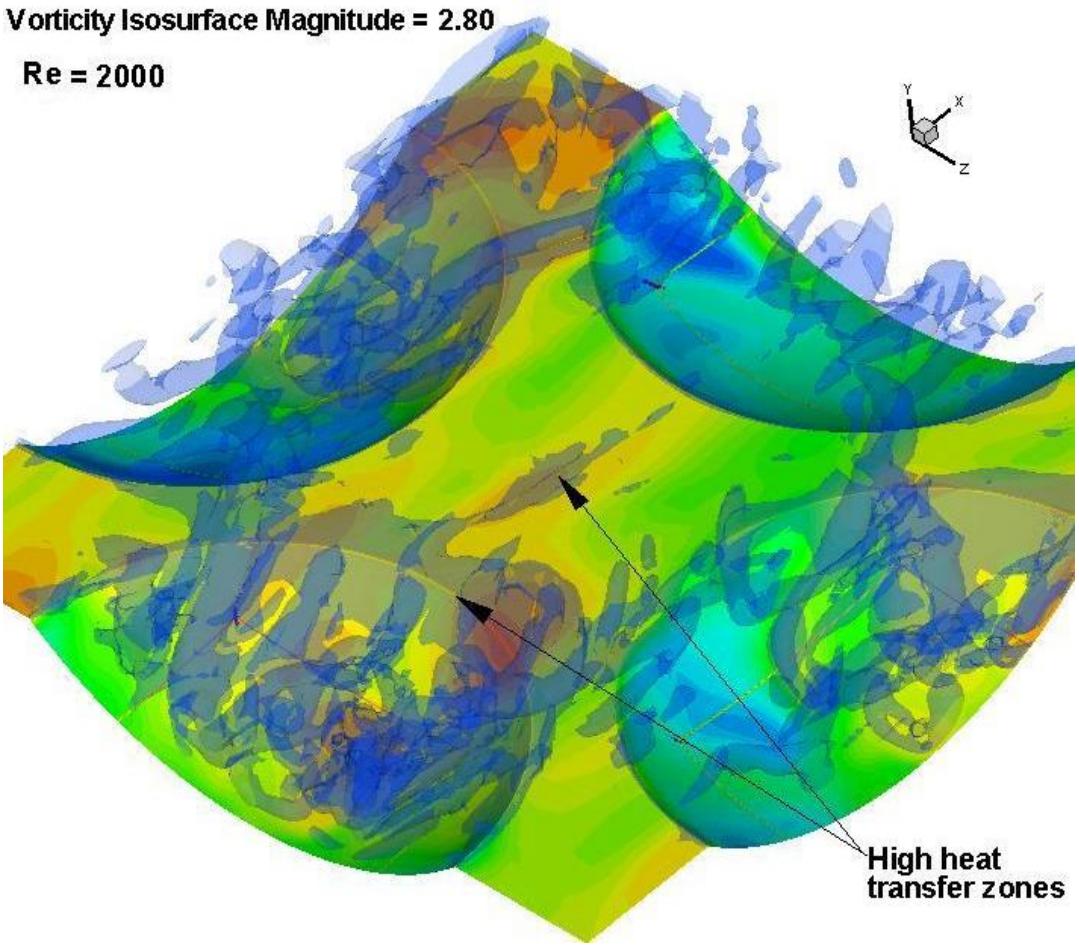

Figure 12. Instantaneous coherent vorticity correlated to heat transfer augmentation.

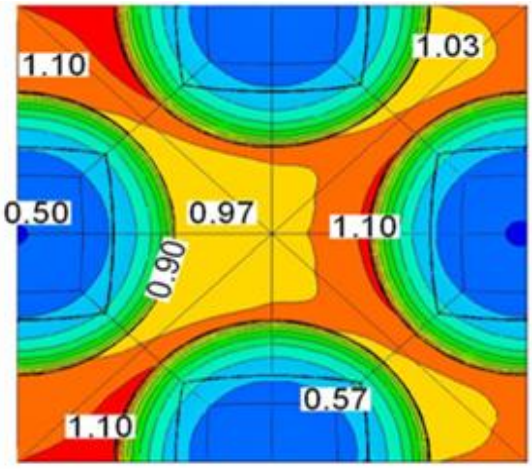

(a) *Re* = 25

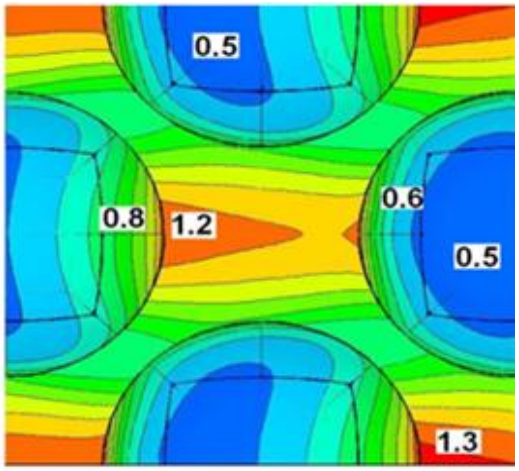

(b) *Re* = 280

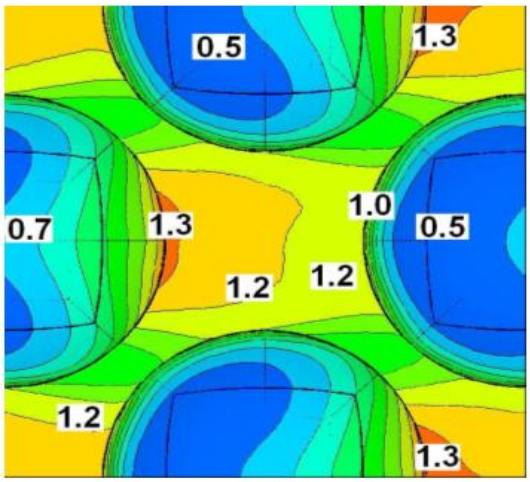

(c) *Re* = 570

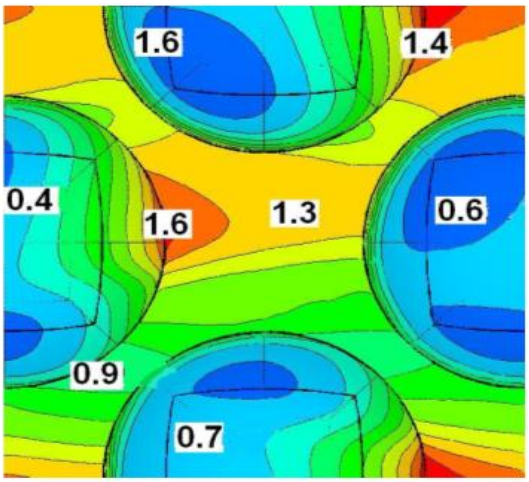

(d) *Re* = 1020

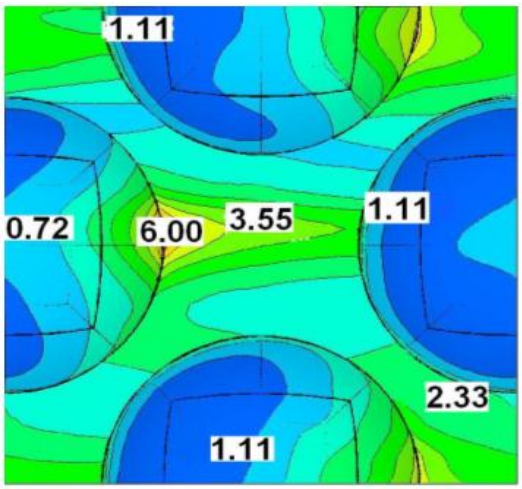

(e) *Re* = 1130

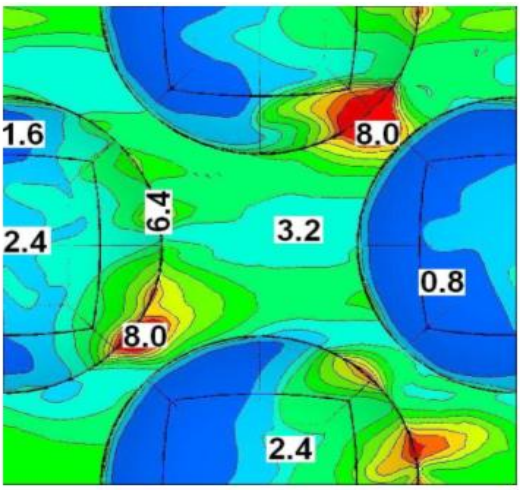

(f) *Re* = 1600

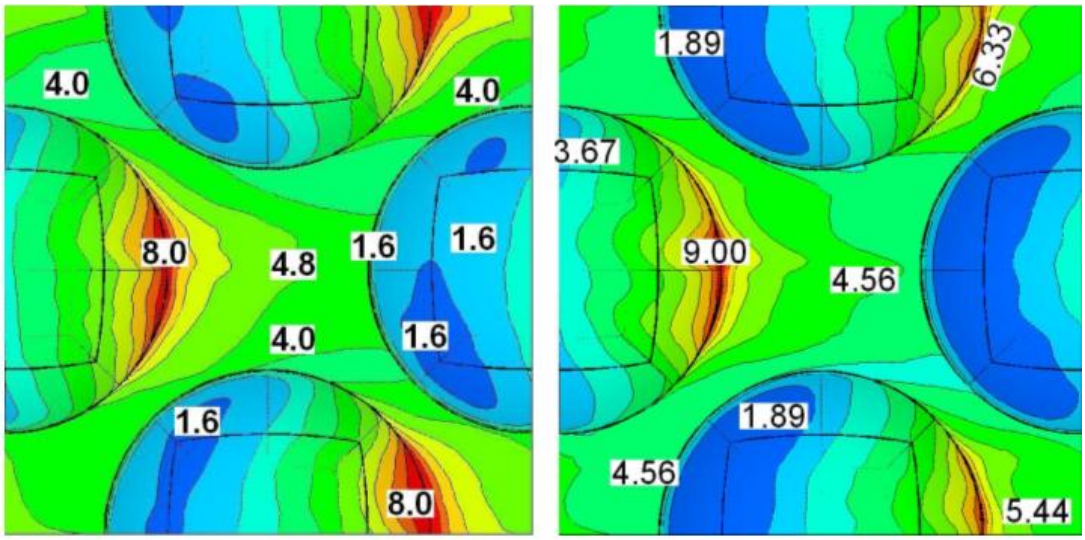

(g) *Re* = 2000 (h) *Re* = 2000t

Figure 13. Nusselt number augmentation ratios at the dimpled surface compared to smooth laminar channel flow.

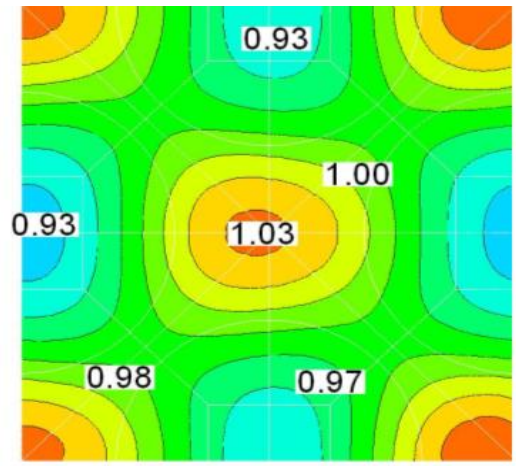

(a) *Re* = 25

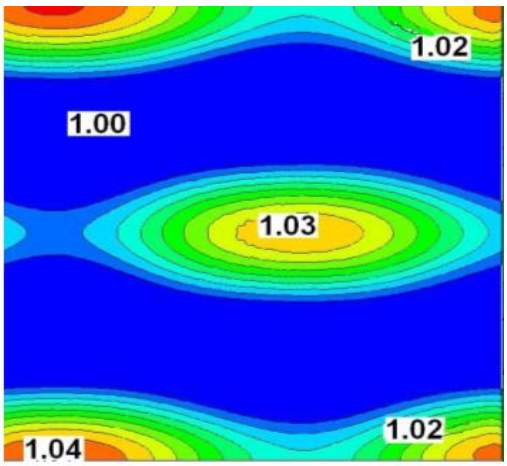

(b) *Re* = 280

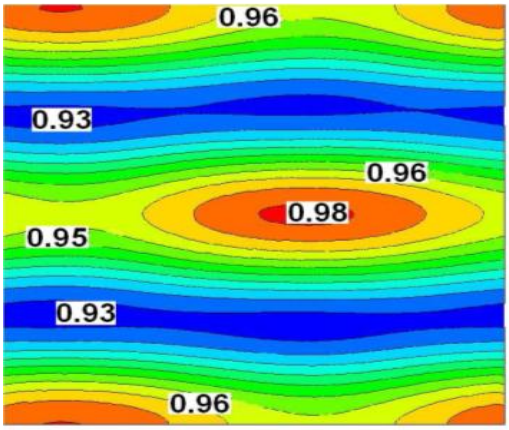

(c) *Re* = 570

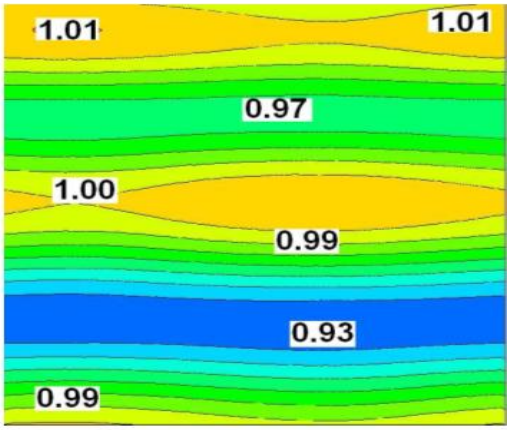

(d) *Re* = 1020

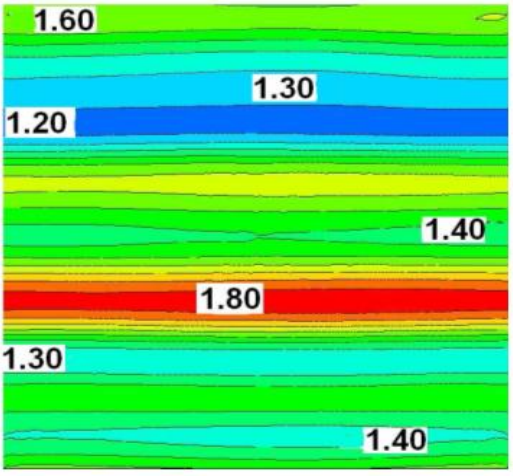

(e) *Re* = 1130

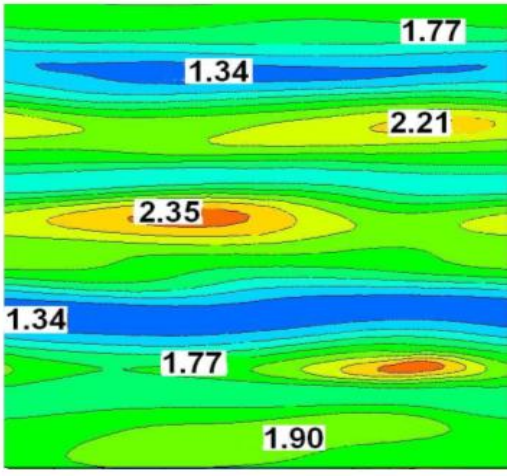

(f) *Re* = 1600

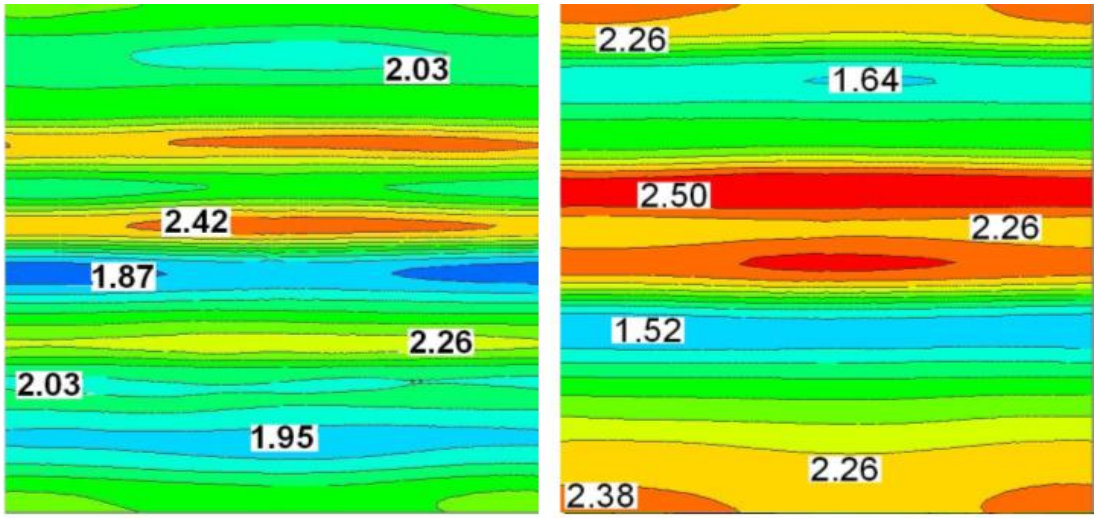

(g) *Re* = 2000 (h) *Re* = 2000t

Figure 14. Nusselt number augmentation ratios on top channel wall compared to smooth laminar channel flow.

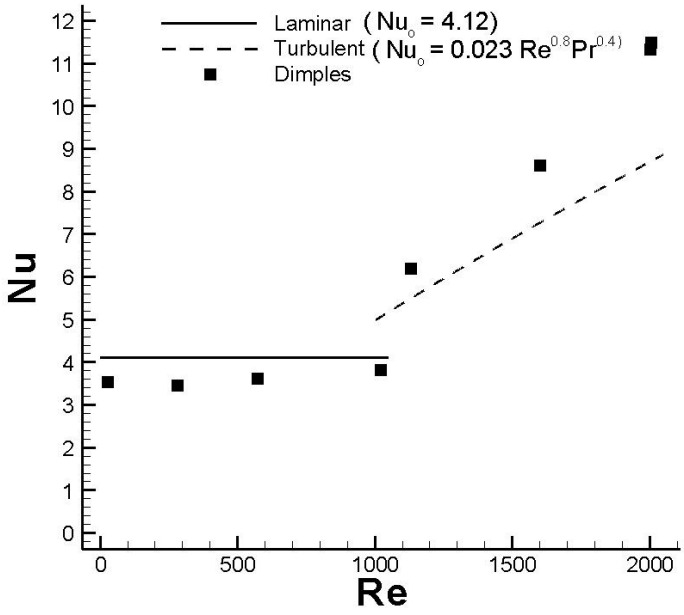

(a)

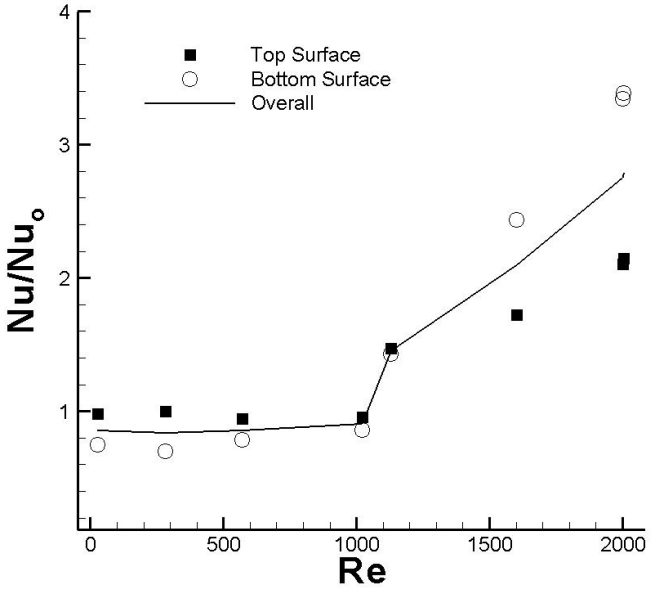

(b)

Figure 15. (a) Predicted overall Nusselt numbers compared to laminar and turbulent correlations. (b) Augmentation ratios for top and bottom surface based on laminar channel flow.

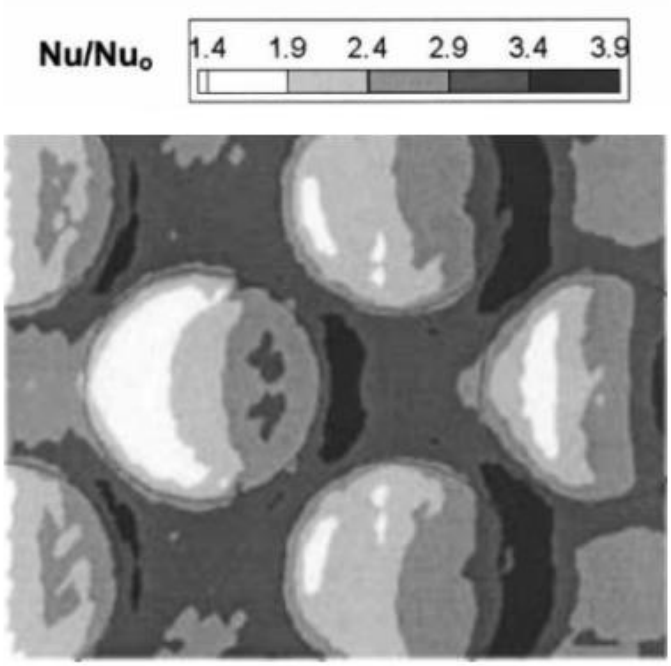

(a)

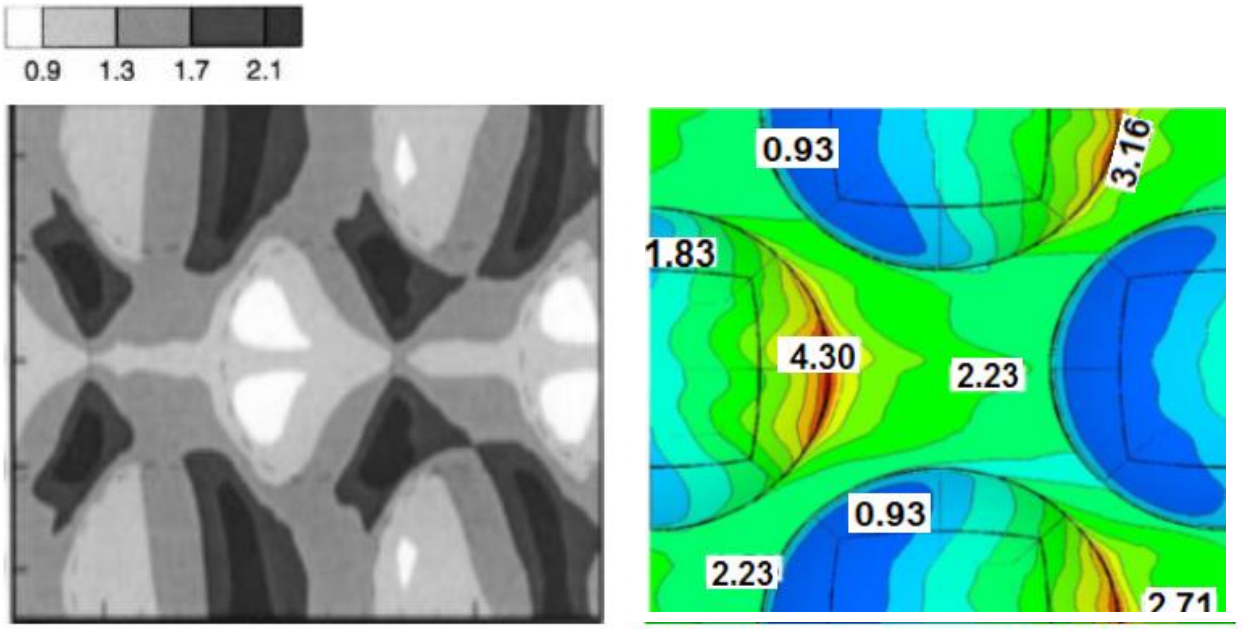

(c)

Figure 16. (a) Experimentally measured surface Nusselt number augmentation for Re = 17,200 from Burgess et al. [2000] (b) Numerically predicted surface Nusselt number augmentation for Re = 17,200 from Park et al. [2002]. (c) Current predictions obtained at Re = 2000 normalized by the Dittus-Boelter correlation.